https://doi.org/10.5194/egusphere-2026-4726
Preprint. Discussion started: 28 August 2026

Precisely dated records of pre-aged terrestrial organic matter release to the western Laptev Sea during the last deglaciation

Tsai-Wen Lin[1,2], Florian Adolphi[1,2,3], Hendrik Grotheer[1,2,3], Jens Hefter[1], Tommaso Tesi[4], Johannes Lachner[5], Stella Winkler[5], Junjie Wu[1], Eduardo Queiroz Alves[6], Gesine Mollenhauer[1,2,3]

[1]Alfred Wegener Institute, Helmholtz Centre for Polar and Marine Research, Marine Geochemistry, 27570 Bremerhaven, Germany

[2]Department of Geosciences, University Bremen, 28334 Bremen, Germany

[3]MARUM Centre for Marine Environmental Sciences, University Bremen, 28334 Bremen, Germany

[4]Institute of Polar Sciences, National Research Council, 40129 Bologna, Italy

[5]Institute of Ion Beam Physics and Materials Research, Helmholtz-Zentrum Dresden-Rossendorf (HZDR), 01328 Dresden, Germany

[6]Programa de pós-graduação em Geoquímica, Instituto de Química, Universidade Federal Fluminense, Niterói, Brazil

Corresponding authors: Tsai-Wen Lin (tsai-wen.lin@awi.de) and Gesine Mollenhauer (gesine.mollenhauer@awi.de)

Highlights

- A deglacial ΔR value of −164 ± 56 ^{14}C yr in the western Laptev Sea is determined by matching marine authigenic ^{10}Be/^{9}Be changes to ice core ^{10}Be fluxes.
- Compound-specific radiocarbon dating of terrestrial biomarkers reveals mobilization of strongly pre-aged materials from thawing permafrost.
- Pre-depositional ^{14}C ages of terrestrial fatty acids indicate varying sources of organic matter between periods of elevated coastal erosion and periods with high river input.
- In the western Laptev Sea, major peat inputs originated from aged permafrost during the last deglaciation.

Abstract

Rapid mobilization of organic carbon from thawing terrestrial permafrost into the Arctic Ocean has been documented for several intervals during the last deglaciation based on marine sediment archives. Assessing the significance of this process for the global carbon cycle requires robust chronological control to better constrain the potential environmental drivers of terrestrial organic carbon mobilization. Identifying the sources of the mobilized terrigenous material is equally critical, as terrestrial permafrost deposits of different ages vary in their potential to release greenhouse gases upon thawing. Motivated by these needs, this study derived a precise age model for a sediment record composed of two cores retrieved from the western Laptev Sea (PS51/154-11 and PS51/159-10) and investigated whether the sources of mobilized permafrost materials during periods of rapid terrestrial permafrost thaw varied over time. This was achieved by aligning ^{10}Be/^{9}Be variations between marine sediment and ice core records, revealing that the age difference between local and global marine reservoir ages (ΔR) was -164 ± 56 ^{14}C yr on the western Laptev Sea shelf and remained relatively stable from the last deglaciation to the present. The previously published radiocarbon-based age-depth models for the two cores were refined using this updated ΔR value, enabling a precise temporal assessment of these records. Radiocarbon ages of terrestrial biomarkers were determined from intervals of maximal terrestrial organic matter delivery recorded in cores PS51/154-11 and PS51/159-10. Compound-specific ^{14}C ages of high molecular weight (n-$C_{28:0}$) fatty acids indicated source variations influenced by transport mechanisms, with a higher contribution of aged material during periods of rapid coastal-eroded terrestrial permafrost mobilization and a dominance of near-surface, younger permafrost during intervals of elevated river discharge. In contrast, mid-chain (n-C_{23}+n-C_{25}) and high molecular weight (n-C_{29}+n-C_{31}) n-alkanes suggested ancient permafrost to be the predominant source for terrestrial inputs to the marine shelf during periods of accelerated land-to-ocean exchange. Our findings on the pre-depositional ^{14}C ages of terrestrial biomarkers highlighted the complexity of permafrost mobilization pathways as captured by different lipid compounds.

Keywords

Last deglaciation, permafrost thaw, $^{10}Be/^{9}Be$, ΔR, compound-specific radiocarbon analysis, CSRA, terrestrial biomarkers, pre-depositional age

1. Introduction

Permafrost, defined as soil that remains below 0 °C for at least two consecutive years (Van Everdingen, 2005), is widely distributed across the circumarctic region (Obu et al., 2019). The persistently low temperature of permafrost facilitates the preservation of organic carbon within it. In Siberia and Alaska, permafrost deposited during the Pleistocene comprises a major carbon pool (Schuur et al., 2015; Strauss et al., 2017), and constitutes an important source of organic matter (OM) to Arctic marginal sea sediments, including those of the Laptev Sea (Karlsson et al., 2011; Vonk et al., 2012; Vonk et al., 2014; Martens et al., 2022). Notably, a large amount of Pleistocene permafrost deposited in Siberia and Alaska is exceptionally ice-rich, making it particularly prone to thaw (Strauss et al., 2017; Strauss et al., 2025). As a result, thawing and degrading of these deposits can release previously freeze-locked carbon into the atmosphere, contributing to an increase in atmospheric greenhouse gases thereby amplifying Arctic warming through positive feedback (Miller et al., 2010; Köhler et al., 2014; Winterfeld et al., 2018; Meyer et al., 2019).

Permafrost from different depth horizons can be mobilized through distinct mechanisms following thaw. Relatively young OM in surface permafrost can be mobilized through increased surface runoff and leaching from the seasonally thawed active layer (Schuur et al., 2008; Schuur et al., 2015). In contrast, aged OM stored in deeper permafrost horizons can be translocated through active layer deepening (Stendel and Christensen, 2002; Gabysheva et al., 2022) or eroded from deeper permafrost via coastal erosion (Overduin et al., 2016; Shadrick et al., 2022), riverbank erosion (Zhang et al., 2022), and thermokarst slumps (Turetsky et al., 2020). The mobilized terrestrial organic matter (terrOM) is eventually transported to and deposited on marginal continental shelves. Determining whether the mobilized terrOM originated from aged or contemporary permafrost sources is crucial for understanding the potential climatic feedback from thawing permafrost. If aged permafrost constitutes the primary source, it implies that more carbon is released from long-term reservoirs, thereby increasing the fast-cycling carbon pool. The difference between the radiocarbon age of terrOM and the age of the surrounding marine sediments at its time of deposition (pre-depositional age) serves as an indicator of the source of terrOM (Winterfeld et al., 2018; Meyer et al., 2019; Wu et al., 2022).

Investigating OM movements from hinterland into the marine shelf during the last deglaciation period (~19−11 kyr BP) offers insights into the mechanisms of permafrost mobilization under accelerated climate warming conditions (Fahl and Stein, 2012; Lambeck et al., 2014; Marcott et al., 2014; Brosius et al., 2021),

https://doi.org/10.5194/egusphere-2026-4726
Preprint. Discussion started: 28 August 2026

of which the trend is comparable to the projected future warming in the IPCC report (Meredith et al., 2019). Several studies have hypothesized that part of the rapid atmospheric CO_2 rise during the last deglaciation (~14.6 kyr BP) and the Preboreal (~11.5 kyr BP) may have originated from the release of aged carbon from thawing permafrost (Köhler et al., 2014; Köhler et al., 2017; Crichton et al., 2016). It has been shown that indeed, sediments in many Arctic locations contain records of distinct maxima in terrOM accumulation, likely derived from thawing permafrost, some of which occurred during the intervals of rapid atmospheric CO_2 rise (Tesi et al., 2016; Winterfeld et al., 2018; Keskitalo et al., 2017; Meyer et al., 2019; Wu et al., 2022; Nogarotto et al., 2023; Lin et al., 2025b; Nicolas et al., 2025). However, precise attribution of the observed peaks to drivers like inland warming or coastal erosion remains difficult, in part due to dating uncertainties.

To better constrain the timing of terrestrial permafrost mobilization and enable comparisons between records, a precise and accurate chronology in marine sediment records is a prerequisite. For most deglacial marine records, chronologies rely on radiocarbon dating, which requires a correction for the local marine reservoir age (MRA). Accurate determination of local MRAs is thus critical but requires chronological constraints that are independent from ^{14}C-dating. Such constraints can be derived from linking variations in the authigenic $^{10}Be/^{9}Be$ ratio in marine sediments to independently dated ^{10}Be-records from ice cores (Nicolas et al., 2024). The atmospheric production rate of the cosmogenic radionuclide ^{10}Be varies with solar activity and Earth's magnetic field strength, due to their influence on the flux of galactic cosmic rays that enter the atmosphere and trigger a secondary particle cascade that produces cosmogenic radionuclides (Lal and Peters, 1967). After production, ^{10}Be arrives in the ocean via wet and dry deposition and is incorporated into the authigenic phase of marine sediments (Bourles et al., 1989; Frank et al., 2009). In contrast, the stable isotope ^{9}Be, is derived from continental rocks and primarily transported to the ocean through river discharge (Bourles et al., 1989; Frank et al., 2009). The authigenic $^{10}Be/^{9}Be$-ratio in marine sediments reflects the $^{10}Be/^{9}Be$ ratio of surrounding seawater at the time of deposition and is thus driven by changes in the cosmogenic production of ^{10}Be and the delivery of ^{9}Be (Von Blanckenburg and Bouchez, 2014; Ollive et al., 2026). Since global fluctuations in atmospheric ^{10}Be production rate also leave imprints in ice cores, aligning ^{10}Be-production-rate signals contained in marine sediments and ice cores can be used to establish a ^{14}C-independent chronology for the marine sediments (e.g., Simon et al., 2020; Nicolas et al., 2024; Loftfield et al., 2025). Combining authigenic $^{10}Be/^{9}Be$ alignment with ^{14}C measurements then allows the estimation of local ^{14}C MRA and the refinement of radiocarbon-based age models (Nicolas et al., 2024).

Previous marine sediment records of Arctic permafrost dynamics primarily focused on regions adjacent to major rivers and may predominantly reflect river-derived signals (e.g., Tesi et al., 2016; Meyer et al., 2019; Wu et al., 2022; Nicolas et al., 2025). In this study, we present two marine sediment core records (PS51/154-11 and PS5/159-10) from the western Laptev Sea shelf, providing insights into the sources and mechanisms of terrestrial permafrost mobilization in areas less influenced by major river discharge. Previous studies on these cores have established a framework including age model studies (Bauch et al., 2001; Taldenkova et al., 2010; Hörner et al., 2016; Lin et al., 2025b), freshwater input history (Taldenkova et al., 2012), and variations in terrOM accumulation rate (Hörner et al., 2016; Lin et al., 2025b). Building on these published datasets, we develop a refined age model based on authigenic $^{10}Be/^{9}Be$ ratios, which allows tying events observed in the sediment to climatic records from ice cores. We further investigate changes in mobilized terrestrial permafrost during the last deglaciation by analyzing the radiocarbon ages of lipid compounds preserved in Laptev Sea shelf sediments. Overall, we aim to offer a more refined perspective on OM release from permafrost at different depth compartments in response to climate

https://doi.org/10.5194/egusphere-2026-4726
Preprint. Discussion started: 28 August 2026

variability, which is crucial for predicting the role of thawing permafrost in the carbon cycle under intensified warming.

2. Study area

Permafrost formed during the late Pleistocene is widely distributed across Siberia and Alaska. These regions remained free of ice sheet cover during the last deglaciation (Hughes et al., 2016), allowing vegetation to grow and become preserved in permafrost soils. This ice- and organic-rich permafrost soil formed during the late Pleistocene is specifically referred to as Yedoma (Strauss et al., 2015; Strauss et al., 2021; Strauss et al., 2022) (Figure 1). Overlying the aged Pleistocene Yedoma is young permafrost soil formed during the Holocene, with modern vegetation on top of these layers.

Terrestrial input from Siberian permafrost regions constitutes the primary OM source to the Laptev Sea, delivered mainly via coastal erosion and river discharge, particularly from the Lena River (Boucsein and Stein, 2000; Günther et al., 2013; Mcclelland et al., 2016; Martens et al., 2022). Annual sediment input and particulate organic contributions from coastal erosion in the Laptev Sea are around 2.5 and 4 times greater than those from river discharge, respectively (Rachold et al., 2000; Stein and Fahl, 2004; Martens et al., 2024). This is because of high coastal erosion rates due to high cliffs, enhanced wave development lead by seasonal sea-ice melting (Rachold et al., 2000; Lantuit et al., 2011), and widespread Quaternary permafrost outcrops along most of the Laptev Sea coastline (Kizyakov et al., 2023). Approximately half of the terrigenous organic carbon deposited on the Laptev Sea shelf is contributed by Pleistocene Yedoma, while the other half is derived from Holocene permafrost soils (Martens et al., 2022). Suspended sediments and freshwater discharged from the Lena River are transported predominantly east- and northward under the influence of local winds (Dmitrenko et al., 1999; Guay et al., 2001), whereas the western Laptev Sea primarily receives water and sediment inputs from the Khatanga River and the Kara Sea (Müller and Stein, 2000).

https://doi.org/10.5194/egusphere-2026-4726
Preprint. Discussion started: 28 August 2026

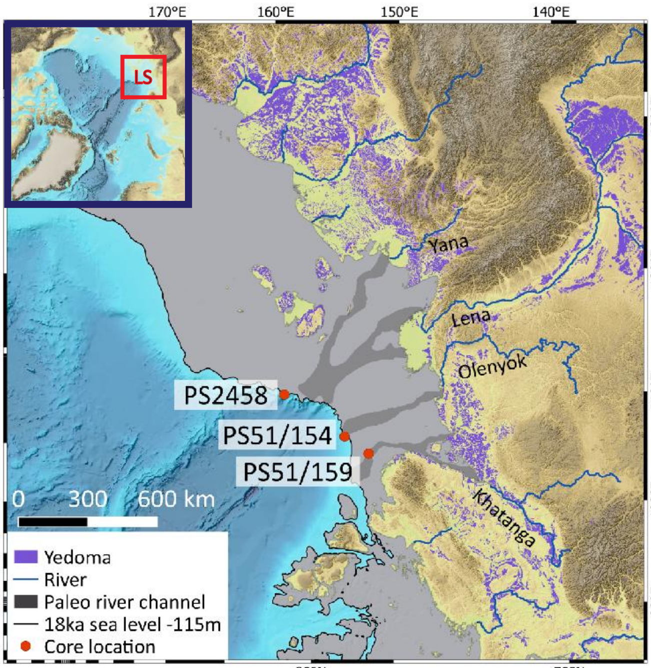

Figure 1. Map of the study area and core locations. The overview map shows the polar projection of the Arctic Ocean and the study area, the Laptev Sea (LS). Red dots indicate the locations of marine sediment cores, including cores PS2458 (Nicolas et al., 2024), PS51/154 (Taldenkova et al., 2012; this study; Lin et al., 2025b), and PS51/159 (Lin et al., 2025b; this study). The grey area indicates the exposed sea shelf at 18 kyr BP, when the sea level was 115 m lower than present (Klemann et al., 2015), assuming the modern bathymetry data approximates (Jakobsson et al., 2012). Dark gray areas highlight paleo river channels (Kleiber and Niessen, 2000). The purple area shows the distribution of the Yedoma domain (Strauss et al., 2016), and dark blue lines mark major rivers (Lehner and Grill, 2013).

The Laptev Sea shelf is characterized by a flat and shallow topography with an average water depth of 50 m, which was exposed during low sea level periods of the last glacial maximum. Several paleo-river channels cut through the shelf and are filled by sediments (Kleiber and Niessen, 2000) (Figure 1). The last deglaciation was marked by several periods of conditions promoting terrestrial permafrost mobilization, including rapid sea-level rise, accelerated inland warming, and reduced sea-ice coverage. In the Laptev Sea, sea level has risen by approximately 115 m from the beginning of the last deglaciation to the present, with two periods of rapid sea-level rise from 14.5 to 13.5 kyr BP and from 11.5 to 10.5 kyr BP (Figure 3c; Klemann et al., 2015), coinciding with global meltwater pulses (Lambeck et al., 2014). Evidence for accelerated inland warming in Siberia was found at 13.2 kyr BP and 10.4 kyr BP (Brosius et al., 2021), and gradual warming was reported for the early Holocene to the mid-Holocene (Andreev et al., 2011). Approximately coeval with inland warming, sea-ice coverage in the Laptev Sea was reconstructed to have decreased (Hörner et al., 2016). Intensified inland warming could drive permafrost thaw and land destabilization (Schuur et al., 2008). Rapid sea-level rise likely accelerated coastal erosion by allowing

https://doi.org/10.5194/egusphere-2026-4726
Preprint. Discussion started: 28 August 2026

waves to reach further inland and erode coastal cliffs (Limber et al., 2018; Shadrick et al., 2022). Reduced winter land-fast sea ice cover results in weaker protection against seawater thermal denudation, wave-driven erosion, and saltwater intrusion into permafrost coastlines (Rachold et al., 2000; Overduin et al., 2016; Nielsen et al., 2020; Irrgang et al., 2022). Due to the broad and shallow shelf of the Laptev Sea, the rate of shelf inundation in this area was highly sensitive to sea-level fluctuations (Bauch et al., 2001; Jakobsson et al., 2012) (Figure 1). Inundation rates began to increase at ~14 kyr BP, and remained high until ~6.5 kyr BP, even though the rate of sea-level rise slowed after 10.5 kyr BP (Figure 3b). These periods of rapid coastal erosion and warming were found to be associated with high sedimentation rates and enhanced terrOM mobilization to the Laptev Sea shelf (Stein and Fahl, 2000; Bauch et al., 2001; Hörner et al., 2016; Lin et al., 2025b) (Figure 3b, c, i).

3. Material and methods

3.1. Material

Kasten cores PS51/154-11 from the upper continental slope (77.276 °N, 120.610 °E, water depth 270 m, abbreviated as PS51/154) and PS51/159-10 from the outer shelf (76.767 °N, 116.032 °E, water depth 60 m, abbreviated as PS51/159) were obtained during the ARK-XIV/1b (PS51 Transdrift-V) expedition in August 1998 aboard the R/V *Polarstern* (Fahrbach, 1998; Kassens, 2016) (Figure 1). The cores were stored at −20 °C and temporarily warmed to 4 °C for subsampling. Sediment samples were collected at 5–10 cm intervals using syringes and analyzed for biomarker contents, as described in Lin et al. (2025b). Based on downcore variations in biomarker contents (Lin et al., 2025b), a second set of larger sediment samples, consisting of slices between 1 and 4 cm thick, was sampled for compound-specific radiocarbon analysis (CSRA). These samples targeted intervals corresponding to periods of maxima and minima in terrOM mass accumulation rates (MAR), as well as depths representative of the early last deglaciation and Holocene periods.

3.2. ^{10}Be and ^{9}Be measurements and ΔR assessment of core PS51/154

Sediments from core PS51/154 were analyzed for authigenic ^{10}Be/^{9}Be ratios to constrain the ΔR (i.e., the difference between local and global marine reservoir ages at the same time) during the last deglaciation, which represents the age difference between local MRA and global MRA included in the marine radiocarbon dating calibration curve, Marine20 (Heaton et al., 2020). Out of the deglaciation period studied here, the time interval between 15 and 10 kyr BP was selected for comparison with the precisely dated ice-core ^{10}Be records, as it was characterized by significant changes in atmospheric ^{10}Be production rates, likely due to changes in solar activity (Adolphi et al., 2017). Based on the age-depth model from Lin et al. (2025b), a subset of 38 sediment samples from the interval between 50.5 and 450.5 cm depth was selected, using the same sample set analyzed for biomarker content. Sediments were leached following the procedure described in Gutjahr et al. (2007), and beryllium was purified following Loftfield et al. (2024). In brief, 1.5 g of freeze-dried, homogenized sediment was first decarbonated with a mixture of sodium acetate and acetic acid. After discarding the supernatant, sediments were subsequently leached with hydroxylamine hydrochloride to extract authigenic ^{10}Be and ^{9}Be. The leachate was then split into two aliquots. One aliquot was used for ^{9}Be measurement via Inductively coupled plasma atomic emission spectroscopy (Thermo Fisher Scientific Inc., ICP-OES-iCAP7400) at the Alfred Wegener Institute (AWI), Bremerhaven. The other aliquot was spiked with ^{9}Be-carrier and further purified following Loftfield et al. (2024). The purified samples were transferred into quartz crucibles, calcined at 900 °C, mixed with Nb-powder, and pressed into copper cathodes for accelerator mass spectrometry (AMS) measurements of

https://doi.org/10.5194/egusphere-2026-4726
Preprint. Discussion started: 28 August 2026

^{10}Be at the DREAMS (DREsden AMS) facility (Lachner et al., 2023). A standard material (SMD-Be-12) was measured as a reference alongside the samples to monitor measurement uncertainties of ^{10}Be (Akhmadaliev et al., 2013). Typical measurement uncertainties were around 5% for ^{9}Be and 3% for ^{10}Be, resulting in an overall uncertainty of 6% for $^{10}Be/^{9}Be$ ratios.

The refined ΔR value for core PS51/154 was estimated following the approach of Nicolas et al. (2024). Authigenic $^{10}Be/^{9}Be$ ratios were first normalized by subtracting a linear regression trend to remove a potential long-term impact of changing contributions of oceanic and riverine beryllium sources (Figure S1c, d). Since ^{9}Be originates from terrestrial sources, long-term variations in riverine input with a low $^{10}Be/^{9}Be$ ratio could influence the $^{10}Be/^{9}Be$ ratios on the shelf during the last deglaciation, when the sea level rise caused the shoreline to progressively move away from the core site. The detrended $^{10}Be/^{9}Be$ ratios were then compared to the average ^{10}Be-fluxes from the Antarctic WAIS-Divide ice core (Sigl et al., 2016; Muschitiello et al., 2019) and GISP2 ice core from Greenland (Finkel and Nishiizumi, 1997; Sinnl et al., 2023). Both ice core records were corrected for climatic influences using linear regression against $\delta^{18}O$ and snow accumulation rates, aligned with the IntCal20 timescale, and averaged (Adolphi and Muscheler, 2016; Sigl et al., 2016; Adolphi et al., 2018). In order to be comparable with the marine $^{10}Be/^{9}Be$ record, a centennial scavenging residence time of ~200 years was applied to the ice core ^{10}Be record following Christl (2007). A beryllium residence time (τ) of 200 years was estimated based on the comparison of the relative variations in $^{10}Be/^{9}Be$ ratios between the ice cores and core PS51/154. (Figure 2a). This value falls within the range of τ values reported from the shallow Lomonosov Ridge but is lower than the average τ (800 years) for ^{10}Be in the deep Arctic Ocean (Frank et al., 2009). A shorter residence time is expected in the shelf area due to higher particle fluxes and shallower water depth in the Laptev Sea shelf compared to the central Arctic Ocean.

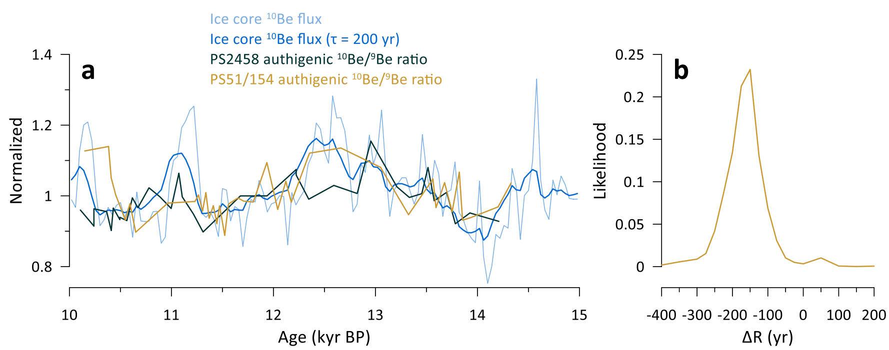

Figure 2. (**a**) Normalized ^{10}Be fluxes from ice cores (Finkel and Nishiizumi, 1997; Sigl et al., 2016; Muschitiello et al., 2019; Sinnl et al., 2023) (pale blue line), and normalized authigenic $^{10}Be/^{9}Be$ ratios from marine sediment core PS2458 (Nicolas et al., 2024) (dark green line), and marine sediment core PS51/154 (this study) (yellow line). The blue line depicts the modeled normalized oceanic ^{10}Be changes from the ice core ^{10}Be data assuming a marine residence time of τ = 200 years. (**b**) Likelihood estimations for the ΔR of core PS51/154 based on the comparison of normalized marine $^{10}Be/^{9}Be$ and ice core ^{10}Be records.

The ^{14}C-based age-depth model for core PS51/154 was initially established based on radiocarbon dating of bivalve shells and foraminifers (Bauch et al., 2001; Taldenkova et al., 2010; Hörner et al., 2016; Lin et

https://doi.org/10.5194/egusphere-2026-4726
Preprint. Discussion started: 28 August 2026

al., 2025b). We used the latest age models published by Lin et al. (2025b), which were calibrated with the Marine20 curve (Heaton et al., 2020) using OxCal 4.4 software (Bronk Ramsey, 2009). An initial ΔR value of −95 ± 61 ^{14}C years was applied, derived from the average local reservoir ages of 5 modern bivalve shells from the Laptev Sea (Bauch et al., 2001), calculated using the Marine20 Marine Reservoir Database (http://calib.org/marine/). This chronology provides the foundation for refining the ΔR value by comparing changes in $^{10}Be/^{9}Be$ ratios between ice core and marine sediment core records. Based on this ^{14}C-based chronology, age models with different ΔR values ranging between −400 and 200 ^{14}C years were calculated in OxCal (Bronk Ramsey, 2009). The resulting $^{10}Be/^{9}Be$ time series were compared to the ice core ^{10}Be-stack using a generalized likelihood function (Christen and Pérez, 2009), the mean ΔR and the standard deviation (1σ) of the likelihood distribution were taken as the refined ΔR estimate and the uncertainty, respectively.

3.3. Compound-specific radiocarbon analysis (CSRA)

Lipid compounds were extracted from marine sediments and purified to assess OM radiocarbon ages derived exclusively from terrestrial sources. Target compounds include mid-chain (C_{23}, C_{25}) *n*-alkanes representing dominant inputs from peat, moss, and aquatic plants, as well as high molecular weight (HMW, or long-chain) (C_{29}, C_{31}) *n*-alkanes and HMW ($C_{28:0}$) fatty acid indicative of terrestrial higher plants (Ficken et al., 2000; Van Dongen et al., 2008; Bianchi and Canuel, 2011). Lipid extractions for CSRA followed the procedure described in Winterfeld et al. (2018). The required sediment weight was calculated from the downcore biomarker contents published by Lin et al. (2025b), aiming to obtain 100 µg C of $C_{28:0}$ fatty acids. Sediments for CSRA were weighed into glass wool thimbles that had been pre-combusted at 450 °C, and the total lipid extracts (TLEs) were obtained using a Soxhlet apparatus with 500 mL dichloromethane + methanol mixture (9:1, *v*/*v*) for at least 48 hours. The TLEs were dried under a stream of nitrogen and split equally into five aliquots for the following steps to ensure complete reactions and prevent overloading of the silica gel columns. Afterward, TLE aliquots were saponified with 5 mL 0.1 M potassium hydroxide (KOH) in a methanol + water mixture (9:1, *v*/*v*) at 80 °C for 2 hours; from there, the neutral lipids (NLs) were extracted with 5 × 5 mL hexane. The remaining TLEs were acidified to pH <2 with 37% HCl, and fatty acids (FAs) were extracted from the acidified solvent with 5 × 5 mL dichloromethane. The hydrocarbon fractions, containing *n*-alkanes, were isolated by eluting the NLs through silica columns with 4 mL of hexane, and the extracts were dried under nitrogen. The FAs were acidified with 37% HCl until pH <2, and methylated with 5 mL methanol of known $\Delta^{14}C$ value. The mixtures were purged with nitrogen to eliminate oxygen. The FAs were then heated to 50 °C for >12 hr, allowing FAs to be methylated into fatty acid methyl esters (FAMEs). After methylation, FAMEs were extracted with 5 × 5 mL hexane and dried under nitrogen. The FAMEs were further eluted through sodium sulfate (Na_2SO_4) and silica gel with 4 mL dichloromethane + hexane mixture (2:1, *v*/*v*) to remove water and polar impurities, respectively. From here, the five aliquots were combined into single FAME and *n*-alkane fractions. A small aliquot of each fraction (1 µL from 8 mL) was quantified using gas chromatograph with a flame ionization detector (GC-FID, Agilent 7890 A) equipped with an Agilent J&W DB-MSs column (60 m × 250 µm × 0.25 µm-thick film).

FAMEs and *n*-alkanes were dissolved in hexane and isolated using preparative capillary gas chromatography (PC-GC, Agilent HP6890N or Agilent HP7890N) with a cooled injection system (CIS, Gerstel) connected to a preparative fraction collector (PFC, Gerstel), equipped with Restek Rxi-1ms fused silica capillary columns (30 m × 530 µm × 1.5 µm-thick film). Retention times of the target compounds were determined in the first PC-GC run of each sample. 5 µL aliquots of the samples were injected per run

https://doi.org/10.5194/egusphere-2026-4726
Preprint. Discussion started: 28 August 2026

until the sample was used up or the accumulated compound mass was sufficient for CSRA analysis. The carbon content and purity of the isolated compounds were determined with a small fraction (1 µL from 1.5 mL) of the sample using a GC-FID (Agilent 7890 A). CSRA analyses were conducted on samples containing a minimum of 40 µg C. Purified compounds were air-dried, transferred to 25 µL tin capsules with dichloromethane, folded, and combusted in an elemental analyzer (EA, Elementar vario Isotope) connected to a gas interface system (GIS). The resulting CO_2 was analyzed using MICADAS for radiocarbon measurements, following the method described in Mollenhauer et al. (2021). CSRA values were reported as $F^{14}C$, which were corrected for carbon introduced during methylation (Douglas et al., 2014) and processing blanks (Wacker and Christl, 2011). Processing blanks were assessed by analyzing modern and fossil laboratory standards processed alongside the samples, following Sun et al. (2020). The estimated background introduced during processing contained 5.5 ± 0.5 µg C with $F^{14}C$ = 0.7632 ± 0.0394 for FAME measurements, and 2.4 ± 0.2 µg C with $F^{14}C$ = 0.3671 ± 0.0296 for *n*-alkane measurements. For samples with low *n*-alkane contents (68 and 142 cm depth in core PS51/154), C_{29} and C_{31} *n*-alkanes were pooled in the tin capsules to ensure sufficient sample mass. For samples with sufficient *n*-alkane content (363.5 cm depth in core PS51/154 and 140 cm depth in core PS51/159), radiocarbon measurements were performed on individual homologues, and weighted average $F^{14}C$ values were calculated based on sample mass.

3.4. *Pre-depositional age correction*

The pre-depositional age, also referred to as the apparent initial age, reflects the time difference between OM biosynthesis and its deposition in marine sediments (Schefuß et al., 2016). This age indicates the intermediate storage period of OM in terrestrial reservoirs prior to deposition as well as the duration of transport to the burial site (Winterfeld et al., 2018; Meyer et al., 2019). Pre-depositional ages for C_{23}+C_{25} *n*-alkanes, C_{29}+C_{31} *n*-alkanes, and $C_{28:0}$ fatty acid were calculated following the method of Schefuß et al. (2016). The $\Delta^{14}C$ value of a compound at the time of deposition ($\Delta^{14}C_{initial}$) was determined using Equation 1, where $F^{14}C$ is the fraction modern from radiocarbon measurements. λ is the decay constant of ^{14}C (1/8267 yr^{-1}), and *t* is the age of deposition, derived from the age-depth model (in yr BP).

$$\Delta^{14}C_{initial} = \left(F^{14}C\, e^{\lambda t} - 1\right) \times 1000\ ‰ \quad (1)$$

Pre-depositional ^{14}C age ($^{14}C\ age_{initial}$) was then calculated using Equation 2. $\Delta^{14}C_{atm.ini}$ is the $\Delta^{14}C$ value in the atmosphere at the time of deposition, interpolated from the IntCal20 curve (Reimer et al., 2020).

$$^{14}C\ age_{initial} = -8033 \times \ln\left(\frac{1 + \frac{\Delta^{14}C_{initial}}{1000}}{1 + \frac{\Delta^{14}C_{atm.ini}}{1000}}\right) \quad (2)$$

4. Results and discussion

4.1. *Comparison of $^{10}Be/^{9}Be$ ratios between marine sediment cores and ice cores*

The authigenic $^{10}Be/^{9}Be$ ratio in core PS51/154 varies between 6.3 × 10^{-9} at/at and 8.6 × 10^{-9} at/at, with a gradual decrease from the lower section of the core (450 cm) to the upper section (50 cm) (Figure S1c). The long-term variation in the authigenic $^{10}Be/^{9}Be$ ratio in core PS51/154 is less pronounced (R^2 = 0.35 for the linear regression trend; Figure S1c) than that observed in core PS2458, which is located on the continental margin of the central Laptev Sea (Nicolas et al., 2024) (Figure 1). This discrepancy can be attributed to the fact that the two cores receive different relative contributions of material from marine and riverine sources (Ollive et al., 2026). During the last deglaciation, core PS2458 was located in close proximity to the Lena River mouth and was predominantly influenced by low $^{10}Be/^{9}Be$ waters discharged from the Lena River ($^{10}Be/^{9}Be$ ratio of ~0.6 ×10^{-8} at/at) (Frank et al., 2009). Today, core PS2458 records a $^{10}Be/^{9}Be$ ratio of ~2×10^{-8} at/at (Nicolas et al., 2024), indicating a substantial contribution of beryllium from the Arctic Ocean, which has a higher $^{10}Be/^{9}Be$ ratio of ~5×10^{-8} at/at (Frank et al., 2009). In contrast, core PS51/154, located on the upper continental slope, is less influenced by beryllium fluxes from the Arctic Ocean, and is characterized by a low $^{10}Be/^{9}Be$ ratio of typical Arctic shelf waters under modern conditions (Ollive et al., 2026). Consequently, the $^{10}Be/^{9}Be$ ratio remained consistently low throughout core PS51/154, with values characteristic of inputs from the Arctic Rivers (<1×10^{-8} at/at; Figure 1) (Frank et al., 2009) and the Laptev Sea shelf (Nicolas et al., 2024; Ollive et al., 2026).

The normalized authigenic $^{10}Be/^{9}Be$ ratio in core PS51/154 exhibits strong comparability to ^{10}Be fluxes in ice core records (Figure 2a), indicating a significant impact of changing ^{10}Be production rates on both records, allowing for their chronological alignment. This correlation enables us to derive the probability density function of ΔR and infer a most likely ΔR of −164 ± 56 ^{14}C yr during the deglaciation period for core PS51/154 (Figure 2b), which corresponds to a local MRA of 341 ± 87 ^{14}C yr during the last deglaciation, based on a global MRA of 505 ± 66 ^{14}C yr during 15−10 kyr BP (Heaton et al., 2020). These findings are consistent with previous estimates of local ΔR of −195 ± 61 ^{14}C yr determined from radiocarbon dating of modern bivalve shells collected from the Laptev Sea shelf (Bauch et al., 2001). Notably, our results suggest that the local ΔR value on the Laptev Sea shelf remained relatively constant from the last deglaciation to the late Holocene. This finding indicates that the localized environmental variability that drive temporal changes in local ΔR values at higher latitudes (Heaton et al., 2023) was likely not substantial in this region.

Changes in the normalized authigenic $^{10}Be/^{9}Be$ ratio in core PS51/154 during the last deglaciation also closely resembles that of core PS2458 from the central Laptev Sea (Figure 2a), although the updated ΔR value for core PS51/154 (−164 ± 56 ^{14}C yr) is about 500 years lower than the ΔR value for core PS2458 (345 ± 60 ^{14}C yr) (Nicolas et al., 2024). To date, all reported reservoir ages for the Laptev Sea are based on radiocarbon dating of modern benthic shells collected from water depths shallower than 50 m (Bauch et al., 2001). Within this dataset, one measurement from near the Lena Delta (water depth 8 m) yields a MRA approximately 500 years higher than those derived from other samples across the Laptev Sea shelf (water depths 25 to 46 m) (Bauch et al., 2001). This offset suggests an additional contribution of aged carbon, likely associated with discharge from the Lena River. During the last deglaciation, core PS2458 was situated near the mouths of the Lena and Yana Rivers, whereas core PS51/154 was located closer to the mouth of Olenyok River (also spelled Olenek River; Kleiber and Niessen, 2000), whose yearly discharge is less than 3% compared to sum of the Lena and Yana Rivers based on modern observation (Milliman et al., 2008; Figure 1). The observed ΔR offset between cores PS2458 and PS51/154 during the deglaciation may therefore reflect varying inputs of pre-aged carbon, with core PS2458 located proximal to the Lena River being more strongly influenced. Alternatively, the high ΔR value in core PS2458 can be attributed to differences in water depth between the coring sites, as core PS2458 was taken from a much deeper site (938 m) compared to core PS51/154 (270 m) (Fütterer, 1994; Fahrbach, 1998). In the absence of independent constrains of modern reservoir ages from the Laptev Sea continental slope, it remains difficult to determine which of these two mechanisms dominates.

With this updated ΔR value (−164 ± 56 ^{14}C yr), new age-depth models for cores PS51/154 and PS51/159 were generated using OxCal 4.4 software (Bronk Ramsey, 2009) with the same microfossil radiocarbon dates as previously used in Lin et al. (2025b) and the Marine20 calibration curve (Heaton et al., 2020) (Figure 3k; Figure S2). The record from core PS51/159 is used to complement the low temporal resolution

https://doi.org/10.5194/egusphere-2026-4726
Preprint. Discussion started: 28 August 2026

of the Holocene section in core PS51/154. Given the close spatial proximity of the two sites and consistency of their biomarker proxy records, we assume comparable marine reservoir age conditions and apply the same updated ΔR value to core PS51/159. Because the difference between the previously used ΔR value (−95 ± 61 ^{14}C yr) and the updated ΔR value (−164 ± 56 ^{14}C yr) is small, the updated age model closely aligns with the previously published age model in Lin et al. (2025b) (Figure S3). According to the revised age model, three periods of peak sedimentation rates were found in core PS51/154 and one peak period was found in core PS51/159, coinciding with intervals of rapid sea level rise and fast shelf inundation (Figure S3). Notably, during these peak sedimentation rate periods, the ^{9}Be content, ^{10}Be content, and ^{10}Be/^{9}Be ratio remained unaltered (Figure S1a, b, c). This stability indicates that the authigenic ^{10}Be/^{9}Be ratio was unaffected by variations in sedimentation rates, confirming its reliability as an independent age control distinct from radiocarbon dating.

4.2. Pre-depositional ^{14}C ages of terrestrial fatty acids reflect events of rapid coastal erosion and high river input

We applied CSRA to $C_{28:0}$ fatty acid to assess shifts in terrOM sources during periods of enhanced terrOM transport to the western Laptev Sea shelf. In cores PS51/154 and PS51/159, pre-depositional ^{14}C ages of $C_{28:0}$ fatty acids exhibited values ranging between 20.1 and 11.55 ^{14}C kyr during periods between the peak terrOM MAR and increased river discharge. The high pre-depositional ^{14}C ages of $C_{28:0}$ fatty acids observed in this study are comparable to, or even higher than, those reported (10−18 kyr) for modern Laptev Sea shelf sediments from areas distant from the Lena River, where the terrOM is derived primarily from coastal erosion rather than riverine sources (Vonk et al., 2014). This similarity in ^{14}C ages suggests that coastal erosion was the dominant terrOM source to cores PS51/154 and PS51/159. Elevated pre-depositional ^{14}C ages (>30 ^{14}C kyr) of $C_{28:0}$ fatty acids in both cores were predominantly recorded during periods of peak terrOM MAR (Table1; Figure 3h, i, yellow boxes), while lower ages of around 4.2 and 10.7 ^{14}C kyr were found between these periods, coinciding with reconstructed intervals of increased river discharge observed from foraminifera assemblage changes (Fig. 3b, blue boxes) (Taldenkova et al., 2012). Based on OM composition and paleoenvironmental information, the three periods of elevated terrOM MAR appear to be linked to different environmental drivers. The first two peak terrOM MAR periods (13.7 and 11.3 kyr BP) are attributed to intensified coastal erosion, whereas the third maximum period in terrOM MAR (10.4 kyr BP) is related to reduced sea-ice coverage and rapid marine transgression (Figure 3b, c) (Lin et al., 2025b). The high pre-depositional ^{14}C ages of $C_{28:0}$ fatty acids during these peak periods of terrOM MAR suggest an increased terrOM influx from aged terrestrial permafrost. However, whether the different environmental causes of these peak terrOM MAR periods mobilized aged terrestrial permafrost through distinct pathways cannot be determined from this dataset. Conversely, during intervals of increased riverine input, the pre-depositional ^{14}C age of $C_{28:0}$ fatty acids decreased (Figure 3h, j, blue boxes), indicating that surface runoff and river discharge transported relatively young $C_{28:0}$ fatty acids to the western Laptev Sea shelf. This younger pre-depositional ^{14}C age is consistent with observed ages of HMW fatty acids ($C_{24:0}$+ $C_{26:0}$+ $C_{28:0}$) deposited near the modern Lena River mouth (5.5 kyr) (Vonk et al., 2014). Thus, changes in the pre-depositional ^{14}C ages of $C_{28:0}$ fatty acids in cores PS51/154 and PS51/159 likely reflect shifts in terrOM sources, specifically between terrOM derived from coastal erosion and river discharge.

During the late Holocene, the pre-depositional ^{14}C ages of $C_{28:0}$ fatty acids in core PS51/159 decreased (Figure 3h). The same phenomenon was also observed in other records from mid- and high-latitude regions of the Northern Hemisphere (Winterfeld et al., 2018; Meyer et al., 2019). Increased vegetation

https://doi.org/10.5194/egusphere-2026-4726
Preprint. Discussion started: 28 August 2026

cover in northern Siberia (Naidina and Bauch, 2001; Andreev et al., 2003) and the stabilization of sea level (Figure 3c; Bauch et al., 2001; Klemann et al., 2015) during the Holocene might have reduced erosion rates and, consequently, the contribution of deep permafrost export, resulting in surface runoff as the predominant source for younger terrOM deposited in the Arctic Ocean (Figure 3h).

https://doi.org/10.5194/egusphere-2026-4726
Preprint. Discussion started: 28 August 2026

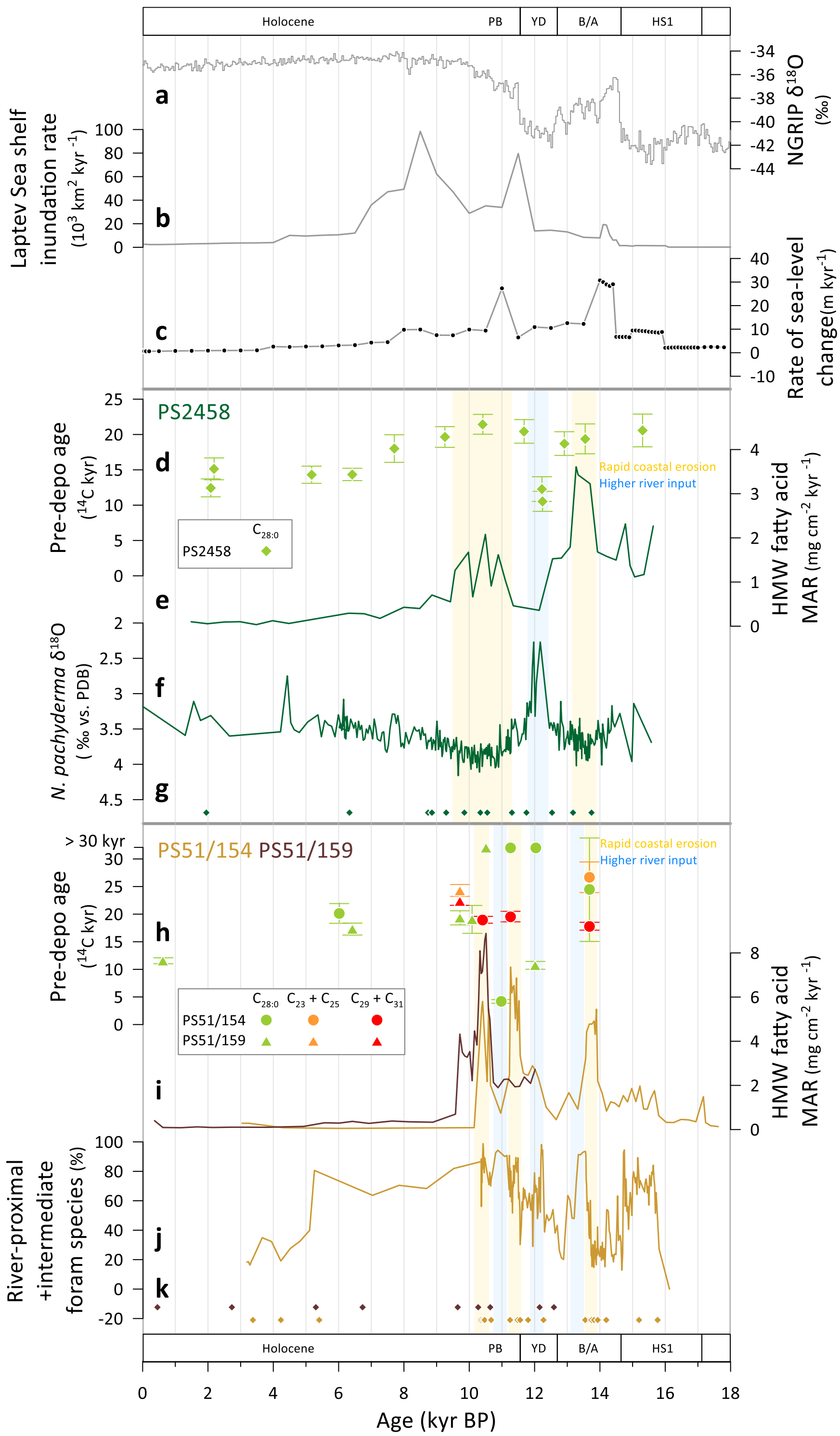

434

https://doi.org/10.5194/egusphere-2026-4726
Preprint. Discussion started: 28 August 2026

Figure 3. Proxy data to constrain terrestrial organic carbon source changes in the Laptev Sea. (**a**) Greenland ice core NGRIP $\delta^{18}O$ values (North Greenland Ice Core Project Members, 2004; Rasmussen et al., 2006). (**b**) Inundation rate of the Laptev Sea shelf, calculated with modern bathymetry (Jakobsson et al., 2012; Klemann et al., 2015). (**c**) rate of sea-level change in the Laptev Sea (Klemann et al., 2015). (**d**) Pre-depositional ^{14}C ages (pre-depo age) of $C_{28:0}$ fatty acid in core PS2458 (Nicolas et al., 2025). (**e**) Changes in terrestrial organic matter (terrOM) mass accumulation rate (MAR), represented by the MAR of HMW fatty acids ($C_{24:0}$+$C_{26:0}$+$C_{28:0}$+$C_{30:0}$) in core PS2458 (Nicolas et al., 2025). (**f**) $\delta^{18}O$ record of planktic foraminifera *N. pachyderma* in core PS2458 (Spielhagen et al., 2005) on an updated age model with $\Delta R = 345 \pm 60$ ^{14}C yr (Nicolas et al., 2024). (**g**) Age-depth model control points from radiocarbon dating of core PS2458 (Nicolas et al., 2025). (**h**) Pre-depositional ^{14}C ages (pre-depo age) of $C_{28:0}$ fatty acids (green), C_{23}+C_{25} *n*-alkanes (orange), and C_{29}+C_{31} *n*-alkanes (red) in cores PS51/154 (circles) and PS51/159 (triangles) (this study). (**i**) Changes in terrestrial organic matter (terrOM) mass accumulation rate (MAR), represented by the MAR of HMW fatty acids ($C_{24:0}$+$C_{26:0}$+$C_{28:0}$+$C_{30:0}$) in cores PS51/154 and PS51/159 (Lin et al., 2025b). (**j**) Relative abundance of river-affected (river-proximal and river-intermediate) benthic foraminifera in core PS51/154 (Taldenkova et al., 2012). (**k**) Age-depth model control points from radiocarbon dating of cores PS51/154 (light brown) and PS51/159 (dark brown) (Bauch et al., 2001; Taldenkova et al., 2010; Hörner et al., 2016; Lin et al., 2025b). Panels **h**–**k** are plotted with an updated age model of $\Delta R = -164 \pm 56$ ^{14}C yr (this study). Yellow bars indicate periods of high terrOM MAR in panel **e** for core PS2458 and in panel **i** for cores PS51/154 and PS51/159. Blue bars indicate periods of enhanced river inputs in panel **f** for core PS2458 and in panel **j** for cores PS51/154 and PS51/159. For display clarity, the uncertainties in the age models of cores PS51/154 and PS51/159 are omitted from this figure, but are provided in Figure S2. Acronyms denote different paleoclimate periods defined by ages derived from the NGRIP $\delta^{18}O$ record: HS1: Heinrich Stadial 1, B/A: Bølling-Allerød, YD: Younger Dryas, PB: Preboreal (Rasmussen et al., 2006; Hodell et al., 2017). A stacked view of the records from cores PS51/154, PS51/159, and PS2458 is shown in Figure S4 to allow for easier comparison across datasets.

4.3. Pre-depositional ^{14}C ages of terrestrial fatty acids from the western and central Laptev Sea shelves

The independent age models using updated ΔR values for core PS2458 from the central Laptev Sea shelf and cores PS51/154 and PS51/159 from the western Laptev Sea shelf provide a valuable framework for aligning terrOM transport events on a sophisticated chronological scale. Enhanced terrOM MAR during the Bølling–Allerød is recorded at both sites, with good agreement in the onset timing of the event (~14–13 kyr BP; yellow bars in Figure 3 and Figure S4). At the beginning of the Holocene (11.7–11.2 kyr BP), a terrOM MAR peak is observed in core PS51/154 but is absent in core PS2458. In the early Holocene (11.3–9.4 kyr BP), core PS2458 exhibits elevated terrOM MAR. This interval overlaps with the peak terrOM MAR recorded in cores PS51/154 and PS51/159 (10.7–10.1 kyr BP), as well as a prolonged phase of elevated terrOM MAR in core PS51/159 between 10.1 and 9.6 kyr BP. Although the onset of increased terrOM MAR periods appear to lag slightly (~0.5 kyr) behind phases of rapid sea-level rise in the Laptev Sea (Figure 3c), considering the age uncertainties on both paleo sea-level modeling and marine sediment age models, these results still support previous hypotheses linking enhanced terrOM fluxes to accelerated coastal erosion driven by rapid sea-level rise (Lin et al., 2025b; Nicolas et al., 2025).

The overall pre-depositional ^{14}C ages of $C_{28:0}$ fatty acids in cores PS51/154 and PS51/159 are comparable to those in core PS2458, indicating similar terrOM sources across the central and western Laptev Sea shelves. This pattern is consistent with observations of bulk OM in marine surface sediments (Lin et al., 2025a). During terrOM MAR peak periods, the pre-depositional ^{14}C ages of $C_{28:0}$ fatty acids in PS51/154

https://doi.org/10.5194/egusphere-2026-4726
Preprint. Discussion started: 28 August 2026

and PS51/159 approach "radiocarbon-dead" values, whereas corresponding ages in core PS2458 show comparatively little variation between high and low terrOM MAR intervals. This larger variability of pre-depositional ages in the western Laptev Sea records suggests a stronger influence of aged terrOM inputs derived from coastal erosion during periods of rapid sea-level rise. Notably, the relatively young pre-depositional ^{14}C age of $C_{28:0}$ fatty acids during the period of increased fresh water input is observed in both records from the western and central Laptev Sea shelves. Taken together, these results indicate that the western Laptev Sea shelf is more sensitive to changes in the composition of terrOM supply between riverine input and coastal erosion, whereas the composition of terrOM input to the central Laptev Sea appears to have remained relatively stable over time despite variations in the rate of terrOM delivery.

4.4. Pre-depositional ^{14}C ages of terrestrial n-alkanes indicate invariant sources

Pre-depositional ^{14}C ages of C_{29}+C_{31} and C_{23}+C_{25} *n*-alkanes were determined to assess changes in terrOM sources across different carbon pools. HMW (C_{29}+C_{31}) *n*-alkanes indicate inputs from higher plants, whereas mid-chain (C_{23}+C_{25}) *n*-alkanes are markers for peat, moss, and aquatic plants (Bianchi and Canuel, 2011). In cores PS51/154 and PS51/159, *n*-alkane pre-depositional ^{14}C ages are only available for a subset of the samples analyzed for fatty acid ages due to their lower abundances (Figure 3h; Table 1). The available ages are all from periods of high terrOM accumulation rates. During these periods, the pre-depositional ^{14}C ages of C_{29}+C_{31} *n*-alkanes were lower than those of $C_{28:0}$ fatty acids (Figure 3h). Previous findings based on modern marine surface sediments from the Siberian Arctic show that hinterlands characterized by less stable permafrost supply older C_{27}+C_{29}+C_{31} *n*-alkanes to adjacent shelves, and these MHW *n*-alkanes are significantly older than the $C_{24:0}$+$C_{26:0}$+$C_{28:0}$ fatty acids analyzed at the same locations (Feng et al., 2015; Gustafsson et al., 2011). In contrast, regions underlain by extensive continuous permafrost yield younger C_{27}+C_{29}+C_{31} *n*-alkanes to the marine shelves, and the age differences between HMW *n*-alkanes and HMW fatty acids are comparatively small or even reversed (Feng et al., 2015; Gustafsson et al., 2011). Based on these previous findings, we hypothesize that the relatively low pre-depositional ^{14}C ages of C_{29}+C_{31} *n*-alkanes compared to $C_{28:0}$ fatty acids in cores PS51/154 and PS51/159 may indicate that even during peak terrOM MAR periods, permafrost stability in the western Laptev Sea inland region remained higher than at present. However, verifying this hypothesis requires further investigation into the relationship between radiocarbon age differences of HMW *n*-alkanes and HMW fatty acids, and their environmental implications.

Table 1. Compound-specific radiocarbon data for high molecular weight (HMW) ($C_{28:0}$) fatty acids, mid-chain (C_{23}+C_{25}) *n*-alkanes, and HMW (C_{29}+C_{31}) *n*-alkanes from cores PS51/154 and PS51/159.

Depth (cm)	Depositional age (cal. kyr BP)	Compound	Mass (µg C)	$F^{14}C$ ±1σ	$\Delta^{14}C_{initial}$ ±1σ (‰)	^{14}C age at deposition ±1σ (kyr)
PS51/154-11						
40.5	6.02	$C_{28:0}$	64	0.042 ± 0.009	−910 ± 19	20.1 ± 1.8
68	10.4	C_{29}+C_{31}	59	0.030 ± 0.002	−890 ± 8	18.9 ± 0.6
124	11	$C_{28:0}$	78	0.181 ± 0.007	−320 ± 32	4.2 ± 0.4
142	11.25	$C_{28:0}$	58	Fossil	Fossil	Fossil
142	11.25	C_{29}+C_{31}	42	0.026 ± 0.003	−900 ± 12	19.5 ± 0.9
273.5	12.05	$C_{28:0}$	64	Fossil	Fossil	Fossil

https://doi.org/10.5194/egusphere-2026-4726
Preprint. Discussion started: 28 August 2026

363.5	13.7	$C_{28:0}$	47	0.011 ± 0.013	−940 ± 66	24.5 ± 9.4
363.5	13.7	C_{23}+C_{25}	86	0.008 ± 0.003	−960 ± 15	26.7 ± 2.8
363.5	13.7	C_{29}+C_{31}	136	0.025 ± 0.002	−870 ± 11	17.8 ± 0.7
PS51/159-10						
12.5	0.62	$C_{28:0}$	40	0.221 ± 0.013	−760 ± 16	11.55 ± 0.55
82.5	6.42	$C_{28:0}$	78	0.058 ± 0.007	−880 ± 17	17.3 ± 1.1
140	9.71	$C_{28:0}$	119	0.030 ± 0.005	−900 ± 16	19.3 ± 1.3
140	9.71	C_{23}+C_{25}	123	0.016 ± 0.002	−950 ± 7	24.2 ± 1.1
140	9.71	C_{29}+C_{31}	146	0.021 ± 0.002	−930 ± 7	22.3 ± 0.8
190	10.1	$C_{28:0}$	59	0.031 ± 0.010	−900 ± 33	19 ± 2.5
280	10.5	$C_{28:0}$	50	Fossil	Fossil	Fossil
401.5	12	$C_{28:0}$	100	0.073 ± 0.006	−690 ± 27	10.7 ± 0.7

Pre-depositional ^{14}C ages of C_{23}+C_{25} *n*-alkanes are only available for two intervals, with 26.7±2.8 ^{14}C kyr during the Bølling-Allerød and 24.2±1.1 ^{14}C kyr during the early Holocene. In both periods, these pre-depositional ^{14}C ages of C_{23}+C_{25} *n*-alkanes exceed those of the HMW *n*-alkanes (Figure 3h, Table 1). Values of the *n*-alkane derived peat index and the $C_{25}/(C_{25}+C_{29})$ *n*-alkane ratio (derived based on Vonk and Gustafsson (2009)) suggest an increase in peatland input to core PS51/154 between 12 and 6.5 kyr BP (Lin et al., 2025b). The high pre-depositional ^{14}C ages of C_{23}+C_{25} *n*-alkanes in cores PS51/154 and PS51/159 during peak terrOM accumulation imply that mobilized peat during those times predominantly originated from ancient permafrost rather than contemporaneously developed peat, despite expanding peatland coverage across the circumarctic during the Preboreal and the early Holocene (Yu et al., 2010; Loisel et al., 2017; Treat et al., 2019; Treat et al., 2021). In Siberia, peat layers are frequently found within Pleistocene permafrost, and thermokarst lake deposits often contain reworked Pleistocene peat (Schwamborn et al., 2002; Hubberten et al., 2004; Strauss et al., 2015; Treat et al., 2019). Thus, the deep peat source can originate from exposed thermokarst slumps that were subsequently mobilized by rapid shelf flooding (Jakobsson et al., 2012; Klemann et al., 2015; Romanovskii et al., 2004) and therefore further support the evidence for the predominant coastal origin of the terrOM accumulating during those times (Figure 3b). On Canadian Arctic shelves, a high pre-depositional ^{14}C age of mid-chain *n*-alkanes has been attributed to petrogenic contributions (Drenzek et al., 2007; Feng et al., 2015), however, this is likely not the case in the Laptev Sea. Although shale outcrops are present in the western Laptev Sea coastlines, particularly in Severnaya Zemlya and the western Taimyr Peninsula (Gee et al., 2006), petrogenic sources are less likely to be the dominant source of C_{23}+C_{25} *n*-alkanes in the western Siberian Shelf. This is supported by the *n*-alkane degradation index (CPI), which exhibits significantly higher values in cores PS51/154 (CPI ranged between 4.8 and 6.6) and PS51/159 (CPI ranged between 4.8 and 6.0; Lin et al., 2025b) than the typical values of petrogenic sources (CPI value around 1; Bray and Evans, 1961) as well as the values observed from the Canadian Arctic shelf (CPI ranged between 1.6 and 2.2; Wu et al., 2022).

5. Conclusions

Both aspects investigated in this study yielded important results for Arctic paleoclimate studies:

1) By comparing the authigenic $^{10}Be/^{9}Be$ ratios in core PS51/154 to ice core ^{10}Be flux, a deglacial ΔR value of −164 ± 56 ^{14}C yr was determined for the western Laptev Sea shelf. This value is consistent within uncertainty with modern ΔR estimations based on radiocarbon dating of locally collected

modern bivalve shells from the Laptev Sea. This consistent value implied that the local ΔR on the Laptev Sea shelf remained remarkably stable from the last deglaciation to the present. However, the ΔR value of core PS51/154 was about 500 ^{14}C yr lower than the deglacial ΔR value of core PS2458 (Nicolas et al., 2024), which was located at the continental margin of the central Laptev Sea and exhibited a much deeper water depth. Our results emphasized that variations in local ΔR, even within the same marginal sea region, could be more substantial than previously expected, and ΔR evaluation for individual sediment cores might be necessary to achieve a precise chronology.

2) The pre-depositional ^{14}C ages of HMW ($C_{28:0}$) fatty acids in cores PS51/154 and PS51/159 reflect different terrOM sources during the last deglaciation, with elevated pre-depositional ^{14}C ages corresponding to periods of intensified coastal erosion and lower pre-depositional ^{14}C ages associated with increased riverine input. Pre-depositional ^{14}C ages of mid-chain (C_{23}+C_{25}) and HMW (C_{29}+C_{31}) *n*-alkanes indicated a predominant contribution from aged permafrost over time, with the latter containing a small younger source. The differences in pre-depositional ^{14}C age change between $C_{28:0}$ fatty acid, C_{23}+C_{25} *n*-alkanes, and C_{29}+C_{31} *n*-alkanes provided indications towards sources and stability of permafrost supplying the terrOM. This study underscored the importance of understanding differences in biomarker mobilization pathways to accurately trace the transport of carbon pools in terrestrial permafrost.

6. Data availability

The data will be uploaded to PANGAEA dataset and once the data are accepted, the dataset DOI will be added here.

7. Author contribution

TWL: Data curation, Formal analysis, Investigation, Visualization, Writing (original draft preparation); FA: Conceptualization, Formal analysis, Funding acquisition, Investigation, Methodology, Project administration, Supervision, Validation, Writing (review and editing); HG: Data curation, Formal analysis, Investigation, Validation, Writing (review and editing); JH: Data curation, Formal analysis, Methodology, Validation, Writing (review and editing); TT: Funding acquisition, Supervision, Writing (review and editing); JL: Data curation, Methodology, Validation, Writing (review and editing); SW: Data curation, Methodology, Validation, Writing (review and editing); JW: Writing (review and editing); EQA: Writing (review and editing); GM: Conceptualization, Funding acquisition, Project administration, Resources, Supervision, Writing (review and editing)

8. Competing interests

One of the co-authors (EQA) is an employee of EGU.

9. Acknowledgments

We thank the captain, the chief scientist, the crew, and the scientific party of the Polarstern Expedition ARK-XIV/1b (PS51 Transdrift-V) during which the cores were collected. We thank Kirsten Fahl and Ruediger Stein for offering coring information. We thank the MICADAS radiocarbon laboratory group members at Alfred Wegener Institute, namely Elizabeth Bonk, Torben Gentz, and Lea Philips, for their help in radiocarbon analyses. We thank Maylin Malter for the ^{10}Be sample preparations. Parts of this research were carried out at the Ion Beam Centre (IBC) at the Helmholtz-Zentrum Dresden-Rossendorf e. V., a

https://doi.org/10.5194/egusphere-2026-4726
Preprint. Discussion started: 28 August 2026

member of the Helmholtz Association. We would like to thank the DREAMS operator team for their assistance with AMS-measurements. We appreciate help from Arnaud Nicolas and Alessio Nogarotto in core subsampling. ChatGPT (version GPT-4) was used in this manuscript to edit grammar and improve sentence fluency.

10. Financial support

This study was supported by the German-Italian partnership project between Alfred Wegener Institute and CNR-ISP on Chronologies for Polar Paleoclimate Archives (PAIGE), funded by the Helmholtz Association (grant PIE-0018). FA is supported through the Helmholtz Association (grant VH-NG 1501).

11. References

Adolphi, F. and Muscheler, R.: Synchronizing the Greenland ice core and radiocarbon timescales over the Holocene – Bayesian wiggle-matching of cosmogenic radionuclide records, Climate of the Past, 12, 15–30, 10.5194/cp-12-15-2016, 2016.

Adolphi, F., Muscheler, R., Friedrich, M., Güttler, D., Wacker, L., Talamo, S., and Kromer, B.: Radiocarbon calibration uncertainties during the last deglaciation: Insights from new floating tree-ring chronologies, Quaternary Science Reviews, 170, 98–108, 10.1016/j.quascirev.2017.06.026, 2017.

Adolphi, F., Bronk Ramsey, C., Erhardt, T., Edwards, R. L., Cheng, H., Turney, C. S. M., Cooper, A., Svensson, A., Rasmussen, S. O., Fischer, H., and Muscheler, R.: Connecting the Greenland ice-core and U/Th timescales via cosmogenic radionuclides: Testing the synchroneity of Dansgaard–Oeschger events, Climate of the Past, 14, 1755–1781, 10.5194/cp-14-1755-2018, 2018.

Akhmadaliev, S., Heller, R., Hanf, D., Rugel, G., and Merchel, S.: The new 6 MV AMS-facility DREAMS at Dresden, Nuclear Instruments and Methods in Physics Research Section B: Beam Interactions with Materials and Atoms, 294, 5–10, 10.1016/j.nimb.2012.01.053, 2013.

Andreev, A. A., Schirrmeister, L., Tarasov, P. E., Ganopolski, A., Brovkin, V., Siegert, C., Wetterich, S., and Hubberten, H.-W.: Vegetation and climate history in the Laptev Sea region (Arctic Siberia) during late Quaternary inferred from pollen records, Quaternary Science Reviews, 30, 2182–2199, 10.1016/j.quascirev.2010.12.026, 2011.

Andreev, A. A., Tarasov, P. E., Siegert, C., Ebel, T., Klimanov, V. A., Melles, M., Bobrov, A. A., Dereviagin, A. Y., Lubinski, D. J., and Hubberten, H. W.: Late Pleistocene and Holocene vegetation and climate on the northern Taymyr Peninsula, Arctic Russia, Boreas, 32, 484–505, 2003.

Bauch, H. A., Mueller-Lupp, T., Taldenkova, E., Spielhagen, R. F., Kassens, H., Grootes, P. M., Thiede, J., Heinemeier, J., and Petryashov, V.: Chronology of the Holocene transgression at the North Siberian margin, Global Planetary Change, 31, 125–139, 10.1016/S0921-8181(01)00116-3., 2001.

Bianchi, T. S. and Canuel, E. A.: Chemical biomarkers in aquatic ecosystems, in: Chemical Biomarkers in Aquatic Ecosystems, Princeton University Press, 10.5670/oceanog.2012.34, 2011.

Boucsein, B. and Stein, R.: Particulate organic matter in surface sediments of the Laptev Sea (Arctic Ocean): Application of maceral analysis as organic-carbon-source indicator, Marine Geology, 162, 573–586, 10.1016/S0025-3227(99)00066-3, 2000.

Bourles, D., Raisbeck, G., and Yiou, F.: 10Be and 9Be in marine sediments and their potential for dating, Geochimica et Cosmochimica Acta, 53, 443–452, 1989.

Bray, E. and Evans, E.: Distribution of n-paraffins as a clue to recognition of source beds, Geochimica et Cosmochimica Acta, 22, 2–15, 1961.

Bronk Ramsey, C.: Bayesian analysis of radiocarbon dates, Radiocarbon, 51, 337–360, 10.1017/s0033822200033865, 2009.

Brosius, L. S., Anthony, K. M. W., Treat, C. C., Lenz, J., Jones, M. C., Bret-Harte, M. S., and Grosse, G.: Spatiotemporal patterns of northern lake formation since the Last Glacial Maximum, Quaternary Science Reviews, 253, 106773, 10.1016/j.quascirev.2020.106773, 2021.

Christl, M.: Sensitivity and response of beryllium-10 in marine sediments to rapid production changes (geomagnetic events): A box model study, Geochemistry, Geophysics, Geosystems, 8, Q09015, 10.1029/2007gc001598, 2007.

Crichton, K. A., Bouttes, N., Roche, D. M., Chappellaz, J., and Krinner, G.: Permafrost carbon as a missing link to explain CO_2 changes during the last deglaciation, Nature Geoscience, 9, 683–686, 10.1038/ngeo2793, 2016.

Dmitrenko, I., Golovin, P., Gribanov, V., and Kassens, H.: Oceanographic causes for transarctic ice transport of river discharge, in: Land-Ocean Systems in the Siberian Arctic, edited by: Kassens, H., Bauch, H. A., Dmitrenko, I. A., Eicken, H., Hubberten, H.-W., Melles, M., Thiede, J., and Timokhov, L. A., Springer Berlin, Heidelberg, 73–92, 10.1007/978-3-642-60134-7_9, 1999.

Douglas, P. M. J., Pagani, M., Eglinton, T. I., Brenner, M., Hodell, D. A., Curtis, J. H., Ma, K. F., and Breckenridge, A.: Pre-aged plant waxes in tropical lake sediments and their influence on the chronology of molecular paleoclimate proxy records, Geochimica et Cosmochimica Acta, 141, 346–364, 10.1016/j.gca.2014.06.030, 2014.

Drenzek, N. J., Montluçon, D. B., Yunker, M. B., Macdonald, R. W., and Eglinton, T. I.: Constraints on the origin of sedimentary organic carbon in the Beaufort Sea from coupled molecular 13C and 14C measurements, Marine Chemistry, 103, 146–162, 10.1016/j.marchem.2006.06.017, 2007.

Fahl, K. and Stein, R.: Modern seasonal variability and deglacial/Holocene change of central Arctic Ocean sea-ice cover: New insights from biomarker proxy records, Earth and Planetary Science Letters, 351-352, 123–133, 10.1016/j.epsl.2012.07.009, 2012.

Fahrbach, E.: FS "Polarstern" ARKTIS XIV/1a+b Russisch-Deutsche Expeditionen, Alfred Wegener Institute for Polar and Marine Research, Bremerhaven, 65, 1998.

Feng, X., Gustafsson, Ö., Holmes, R. M., Vonk, J. E., van Dongen, B. E., Semiletov, I. P., Dudarev, O. V., Yunker, M. B., Macdonald, R. W., Wacker, L., Montluçon, D. B., and Eglinton, T. I.: Multimolecular tracers of terrestrial carbon transfer across the pan-Arctic: 14C characteristics of sedimentary carbon components and their environmental controls, Global Biogeochemical Cycles, 29, 1855–1873, 10.1002/2015gb005204, 2015.

Ficken, K. J., Li, B., Swain, D., and Eglinton, G.: An n-alkane proxy for the sedimentary input of submerged/floating freshwater aquatic macrophytes, Organic Geochemistry, 31, 745–749, 2000.

Finkel, R. C. and Nishiizumi, K.: Beryllium 10 concentrations in the Greenland Ice Sheet Project 2 ice core from 3–40 ka, Journal of Geophysical Research: Oceans, 102, 26699–26706, 10.1029/97jc01282, 1997.

Frank, M., Porcelli, D., Andersson, P., Baskaran, M., Björk, G., Kubik, P. W., Hattendorf, B., and Guenther, D.: The dissolved Beryllium isotope composition of the Arctic Ocean, Geochimica et Cosmochimica Acta, 73, 6114–6133, 10.1016/j.gca.2009.07.010, 2009.

Fütterer, D. K.: The Expedition ARCTIC '93, leg ARK-IX/4 of RV "Polarstern" 1993, Alfred Wegener Institute for Polar and Marine Research, Bremerhaven, 336, 10.2312/BzP_0149_1994, 1994.

Gabysheva, O. I., Gabyshev, V. A., Barinova, S., Yakshina, I. A., and Pavlov, I. S.: Influence of the thickness of the seasonally thawed layer of permafrost in the Eastern Siberia catchments on the content of organic matter in river waters, Hydrobiology, 1, 243–251, 10.3390/hydrobiology1020018, 2022.

Gee, D. G., Bogolepova, O. K., and Lorenz, H.: The Timanide, Caledonide and Uralide orogens in the Eurasian high Arctic, and relationships to the palaeo-continents Laurentia, Baltica and Siberia, Geological Society, London, Memoirs, 32, 507–520, 10.1144/gsl.Mem.2006.032.01.31, 2006.

Guay, C. K., Falkner, K. K., Muench, R. D., Mensch, M., Frank, M., and Bayer, R.: Wind-driven transport pathways for Eurasian Arctic river discharge, Journal of Geophysical Research, 106, 11469–11480, 10.1029/2000JC000261, 2001.

https://doi.org/10.5194/egusphere-2026-4726
Preprint. Discussion started: 28 August 2026

Günther, F., Overduin, P. P., Sandakov, A. V., Grosse, G., and Grigoriev, M. N.: Short- and long-term thermo-erosion of ice-rich permafrost coasts in the Laptev Sea region, Biogeosciences, 10, 4297–4318, 10.5194/bg-10-4297-2013, 2013.
Gustafsson, Ö., van Dongen, B. E., Vonk, J. E., Dudarev, O. V., and Semiletov, I. P.: Widespread release of old carbon across the Siberian Arctic echoed by its large rivers, Biogeosciences, 8, 1737–1743, 10.5194/bg-8-1737-2011, 2011.
Gutjahr, M., Frank, M., Stirling, C. H., Klemm, V., Van de Flierdt, T., and Halliday, A. N.: Reliable extraction of a deepwater trace metal isotope signal from Fe-Mn oxyhydroxide coatings of marine sediments, Chemical Geology, 242, 351–370, 2007.
Heaton, T. J., Bard, E., Bronk Ramsey, C., Butzin, M., Hatté, C., Hughen, K. A., Köhler, P., and Reimer, P. J.: A response to community questions on the Marine20 radiocarbon age calibration curve: Marine reservoir ages and the calibration of 14C samples from the oceans, Radiocarbon, 65, 247–273, 10.1017/rdc.2022.66, 2023.
Heaton, T. J., Köhler, P., Butzin, M., Bard, E., Reimer, R. W., Austin, W. E. N., Bronk Ramsey, C., Grootes, P. M., Hughen, K. A., Kromer, B., Reimer, P. J., Adkins, J., Burke, A., Cook, M. S., Olsen, J., and Skinner, L. C.: Marine20—The marine radiocarbon age calibration curve (0–55,000 cal BP), Radiocarbon, 62, 779–820, 10.1017/rdc.2020.68, 2020.
Hodell, D. A., Nicholl, J. A., Bontognali, T. R. R., Danino, S., Dorador, J., Dowdeswell, J. A., Einsle, J., Kuhlmann, H., Martrat, B., Mleneck-Vautravers, M. J., Rodríguez-Tovar, F. J., and Röhl, U.: Anatomy of Heinrich Layer 1 and its role in the last deglaciation, Paleoceanography, 32, 284–303, 10.1002/2016pa003028, 2017.
Hörner, T., Stein, R., Fahl, K., and Birgel, D.: Post-glacial variability of sea ice cover, river run-off and biological production in the western Laptev Sea (Arctic Ocean)–A high-resolution biomarker study, Quaternary Science Reviews, 143, 133–149, 10.1016/j.quascirev.2016.04.011, 2016.
Hubberten, H. W., Andreev, A., Astakhov, V. I., Demidov, I., Dowdeswell, J. A., Henriksen, M., Hjort, C., Houmark-Nielsen, M., Jakobsson, M., Kuzmina, S., Larsen, E., Lunkka, J. P., Lysa, A., Mangerud, J., Möller, P., Saarnisto, M., Schirrmeister, L., Sher, A. V., Siegert, C., Siegert, M. J., and Svendsen, J. I.: The periglacial climate and environment in northern Eurasia during the Last Glaciation, Quaternary Science Reviews, 23, 1333–1357, 10.1016/j.quascirev.2003.12.012, 2004.
Hughes, A. L., Gyllencreutz, R., Lohne, Ø. S., Mangerud, J., and Svendsen, J. I.: The last Eurasian ice sheets–a chronological database and time-slice reconstruction, DATED-1, Boreas, 45, 1–45, 2016.
Irrgang, A. M., Bendixen, M., Farquharson, L. M., Baranskaya, A. V., Erikson, L. H., Gibbs, A. E., Ogorodov, S. A., Overduin, P. P., Lantuit, H., Grigoriev, M. N., and Jones, B. M.: Drivers, dynamics and impacts of changing Arctic coasts, Nature Reviews Earth & Environment, 3, 39–54, 10.1038/s43017-021-00232-1, 2022.
Jakobsson, M., Mayer, L., Coakley, B., Dowdeswell, J. A., Forbes, S., Fridman, B., Hodnesdal, H., Noormets, R., Pedersen, R., and Rebesco, M.: The international bathymetric chart of the Arctic Ocean (IBCAO) version 3.0, Geophysical Research Letters, 39, 10.1029/2012GL052219, 2012.
Karlsson, E. S., Charkin, A., Dudarev, O., Semiletov, I., Vonk, J. E., Sánchez-García, L., Andersson, A., and Gustafsson, Ö.: Carbon isotopes and lipid biomarker investigation of sources, transport and degradation of terrestrial organic matter in the Buor-Khaya Bay, SE Laptev Sea, Biogeosciences, 8, 1865–1879, 10.5194/bg-8-1865-2011, 2011.
Kassens, H.: Station list and links to master tracks in different resolutions of POLARSTERN cruise ARK-XIV/1b, Tiksi - Tromsø, 1998-07-28 - 1998-08-28, PANGAEA [dataset], 10.1594/PANGAEA.858867, 2016.
Keskitalo, K., Tesi, T., Bröder, L., Andersson, A., Pearce, C., Sköld, M., Semiletov, I. P., Dudarev, O. V., and Gustafsson, Ö.: Sources and characteristics of terrestrial carbon in Holocene-scale sediments of the East Siberian Sea, Climate of the Past, 13, 1213–1226, 10.5194/cp-13-1213-2017, 2017.

https://doi.org/10.5194/egusphere-2026-4726
Preprint. Discussion started: 28 August 2026

Kizyakov, A. I., Ermolov, A. A., Baranskaya, A. V., and Grigoriev, M. N.: Morphodynamic types of the Laptev Sea coast: A review, Land, 12, 1141, 2023.

Kleiber, H. P. and Niessen, F.: Variations of continental discharge pattern in space and time: Implications from the Laptev Sea continental margin, Arctic Siberia, International Journal of Earth Sciences, 89, 605–616, 10.1007/s005310000130, 2000.

Klemann, V., Heim, B., Bauch, H. A., Wetterich, S., and Opel, T.: Sea-level evolution of the Laptev Sea and the East Siberian Sea since the last glacial maximum, Arktos, 1, 10.1007/s41063-015-0004-x, 2015.

Köhler, P., Knorr, G., and Bard, E.: Permafrost thawing as a possible source of abrupt carbon release at the onset of the Bølling–Allerød, Nature Communications, 5, 5520, 10.1038/ncomms6520, 2014.

Köhler, P., Nehrbass-Ahles, C., Schmitt, J., Stocker, T. F., and Fischer, H.: A 156 kyr smoothed history of the atmospheric greenhouse gases CO2, CH4, and N2O and their radiative forcing, Earth System Science Data, 9, 363–387, 10.5194/essd-9-363-2017, 2017.

Lachner, J., Rugel, G., Vivo Vilches, C., Koll, D., Stübner, K., Winkler, S., and Wallner, A.: Optimization of 10Be measurements at the 6 MV AMS facility DREAMS, Nuclear Instruments and Methods in Physics Research Section B: Beam Interactions with Materials and Atoms, 535, 29–33, 10.1016/j.nimb.2022.11.008, 2023.

Lal, D. and Peters, B.: Cosmic ray produced radioactivity on the Earth, in: Kosmische Strahlung II/cosmic rays II, Springer, 551–612, 1967.

Lambeck, K., Rouby, H., Purcell, A., Sun, Y., and Sambridge, M.: Sea level and global ice volumes from the Last Glacial Maximum to the Holocene, Proceedings of the National Academy of Sciences of the United States of America, 111, 15296–15303, 10.1073/pnas.1411762111, 2014.

Lantuit, H., Atkinson, D., Overduin, P. P., Grigoriev, M., Rachold, V., Grosse, G., and Hubberten, H.-W.: Coastal erosion dynamics on the permafrost-dominated Bykovsky Peninsula, north Siberia, 1951–2006, Polar Research, 30, 7341, 10.3402/polar.v30i0.7341, 2011.

Lehner, B. and Grill, G.: Global river hydrography and network routing: Baseline data and new approaches to study the world's large river systems, Hydrological Processes, 27, 2171–2186, 2013.

Limber, P. W., Barnard, P. L., Vitousek, S., and Erikson, L. H.: A model ensemble for projecting multidecadal coastal cliff retreat during the 21st century, Journal of Geophysical Research: Earth Surface, 123, 1566–1589, 10.1029/2017jf004401, 2018.

Lin, T. W., Nehrke, G., Grotheer, H., Koch, B. P., Meyer, H., Ruben, M., Stein, R., Strauss, J., Tesi, T., and Mollenhauer, G.: Holocene Terrestrial Permafrost Contributes More Highly Reactive Organic Matter to the Laptev Sea Shelf Than Pleistocene Permafrost, Journal of Geophysical Research: Biogeosciences, 130, 10.1029/2025jg008872, 2025a.

Lin, T. W., Tesi, T., Hefter, J., Grotheer, H., Wollenburg, J., Adolphi, F., Bauch, H. A., Nogarotto, A., Müller, J., and Mollenhauer, G.: Environmental controls of rapid terrestrial organic matter mobilization to the western Laptev Sea since the Last Deglaciation, Climate of the Past, 21, 753–772, 10.5194/cp-21-753-2025, 2025b.

Loftfield, J., Lachner, J., Malter, M., Stübner, K., and Adolphi, F.: A simple method of purifying authigenic 10Be from sediments for AMS-analysis, Nuclear Instruments and Methods in Physics Research Section B: Beam Interactions with Materials and Atoms, 547, 10.1016/j.nimb.2023.165179, 2024.

Loftfield, J., Nowaczyk, N., Lembke-Jene, L., Frederichs, T., Lachner, J., Lamy, F., Rugel, G., Stübner, K., and Adolphi, F.: Constraints on the use of cosmogenic beryllium isotopes for synchronizing marine sediments and ice cores, Earth and Planetary Science Letters, 671, 10.1016/j.epsl.2025.119665, 2025.

Loisel, J., van Bellen, S., Pelletier, L., Talbot, J., Hugelius, G., Karran, D., Yu, Z., Nichols, J., and Holmquist, J.: Insights and issues with estimating northern peatland carbon stocks and fluxes since the Last Glacial Maximum, Earth-Science Reviews, 165, 59–80, 2017.

Marcott, S. A., Bauska, T. K., Buizert, C., Steig, E. J., Rosen, J. L., Cuffey, K. M., Fudge, T. J., Severinghaus, J. P., Ahn, J., Kalk, M. L., McConnell, J. R., Sowers, T., Taylor, K. C., White, J. W., and Brook, E. J.:

https://doi.org/10.5194/egusphere-2026-4726
Preprint. Discussion started: 28 August 2026

Centennial-scale changes in the global carbon cycle during the last deglaciation, Nature, 514, 616–619, 10.1038/nature13799, 2014.

Martens, J., Wild, B., Semiletov, I., Dudarev, O. V., and Gustafsson, Ö.: Circum-Arctic release of terrestrial carbon varies between regions and sources, Nature Communications, 13, 5858, 10.1038/s41467-022-33541-0, 2022.

Martens, J., Tesi, T., Rusakov, V., Semiletov, I., Dudarev, O., and Gustafsson, Ö.: Off-shelf transport and biogeochemical cycling of terrestrial organic carbon along the East Siberian continental margin, Global Biogeochemical Cycles, 38, e2024GB008104, 10.1029/2024gb008104, 2024.

McClelland, J. W., Holmes, R. M., Peterson, B. J., Raymond, P. A., Striegl, R. G., Zhulidov, A. V., Zimov, S. A., Zimov, N., Tank, S. E., Spencer, R. G. M., Staples, R., Gurtovaya, T. Y., and Griffin, C. G.: Particulate organic carbon and nitrogen export from major Arctic rivers, Global Biogeochemical Cycles, 30, 629–643, 10.1002/2015gb005351, 2016.

Meredith, M., Sommerkorn, M., Cassotta, S., Derksen, C., Ekaykin, A., Hollowed, A., Kofinas, G., Mackintosh, A., Melbourne-Thomas, J., Muelbert, M. M. C., Ottersen, G., Pritchard, H., and Schuur, E. A. G.: Polar regions, in: IPCC Special Report on the Ocean and Cryosphere in a Changing Climate, edited by: H.-O. Pörtner, D.C. Roberts, V. Masson-Delmotte, P. Zhai, M. Tignor, E. Poloczanska, K. Mintenbeck, A. Alegría, M. Nicolai, A. Okem, J. Petzold, B. Rama, and Weyer, N. M., Cambridge University Press, Cambridge, UK and New York, NY, USA, 203–320, 10.1017/9781009157964.005, 2019.

Meyer, V. D., Hefter, J., Köhler, P., Tiedemann, R., Gersonde, R., Wacker, L., and Mollenhauer, G.: Permafrost-carbon mobilization in Beringia caused by deglacial meltwater runoff, sea-level rise and warming, Environmental Research Letters, 14, 085003, 10.1088/1748-9326/ab2653, 2019.

Miller, G. H., Alley, R. B., Brigham-Grette, J., Fitzpatrick, J. J., Polyak, L., Serreze, M. C., and White, J. W. C.: Arctic amplification: Can the past constrain the future?, Quaternary Science Reviews, 29, 1779–1790, 10.1016/j.quascirev.2010.02.008, 2010.

Milliman, J. D., Farnsworth, K. L., Jones, P. D., Xu, K. H., and Smith, L. C.: Climatic and anthropogenic factors affecting river discharge to the global ocean, 1951–2000, Global and Planetary Change, 62, 187–194, 10.1016/j.gloplacha.2008.03.001, 2008.

Mollenhauer, G., Grotheer, H., Gentz, T., Bonk, E., and Hefter, J.: Standard operation procedures and performance of the MICADAS radiocarbon laboratory at Alfred Wegener Institute (AWI), Germany, Nuclear Instruments and Methods in Physics Research Section B: Beam Interactions with Materials and Atoms, 496, 45–51, 10.1016/j.nimb.2021.03.016, 2021.

Müller, C. and Stein, R.: Variability of fluvial sediment supply to the Laptev Sea continental margin during Late Weichselian to Holocene times: Implications from clay-mineral records, International Journal of Earth Sciences, 89, 592–604, 10.1007/s005310000112, 2000.

Muschitiello, F., D'Andrea, W. J., Schmittner, A., Heaton, T. J., Balascio, N. L., deRoberts, N., Caffee, M. W., Woodruff, T. E., Welten, K. C., Skinner, L. C., Simon, M. H., and Dokken, T. M.: Deep-water circulation changes lead North Atlantic climate during deglaciation, Nature Communications, 10, 1272, 10.1038/s41467-019-09237-3, 2019.

Naidina, O. D. and Bauch, H. A.: A Holocene pollen record from the Laptev Sea shelf, northern Yakutia, Global Planetary Change, 31, 141–153, 2001.

Nicolas, A., Hefter, J., Grotheer, H., Tesi, T., Stein, R., Nogarotto, A., Alves, E. Q., and Mollenhauer, G.: Delivery of aged terrestrial organic matter to the Laptev Sea during the last deglaciation, Climate of the Past, 21, 2579–2599, 10.5194/cp-21-2579-2025, 2025.

Nicolas, A., Mollenhauer, G., Lachner, J., Stübner, K., Malter, M., Wollenburg, J., Grotheer, H., and Adolphi, F.: Precise dating of deglacial Laptev Sea sediments via 14C and authigenic 10Be/9Be – assessing local 14C reservoir ages, Climate of the Past, 20, 2617–2628, 10.5194/cp-20-2617-2024, 2024.

https://doi.org/10.5194/egusphere-2026-4726
Preprint. Discussion started: 28 August 2026

Nielsen, D. M., Dobrynin, M., Baehr, J., Razumov, S., and Grigoriev, M.: Coastal erosion variability at the southern Laptev Sea linked to winter sea ice and the Arctic Oscillation, Geophysical Research Letters, 47, e2019GL086876, 10.1029/2019gl086876, 2020.

Nogarotto, A., Noormets, R., Chauhan, T., Mollenhauer, G., Hefter, J., Grotheer, H., Belt, S., Colleoni, F., Muschitiello, F., Capotondi, L., Pellegrini, C., and Tesi, T.: Coastal permafrost was massively eroded during the Bølling-Allerød warm period, Communications Earth & Environment, 4, 350, https://doi.org/10.1038/s43247-023-01013-y, 2023.

North Greenland Ice Core Project members: High-resolution record of Northern Hemisphere climate extending into the last interglacial period Nature, 431, 147–151, 2004.

Obu, J., Westermann, S., Bartsch, A., Berdnikov, N., Christiansen, H. H., Dashtseren, A., Delaloye, R., Elberling, B., Etzelmüller, B., Kholodov, A., Khomutov, A., Kääb, A., Leibman, M. O., Lewkowicz, A. G., Panda, S. K., Romanovsky, V., Way, R. G., Westergaard-Nielsen, A., Wu, T., Yamkhin, J., and Zou, D.: Northern Hemisphere permafrost map based on TTOP modelling for 2000–2016 at 1 km2 scale, Earth-Science Reviews, 193, 299–316, 10.1016/j.earscirev.2019.04.023, 2019.

Ollive, A., Geibert, W., Matthiessen, J., Alscher, M., Frank, M., Lachner, J., Stübner, K., and Adolphi, F.: Processes controlling the authigenic 10Be/9Be ratio in the Arctic Ocean, Geochimica et Cosmochimica Acta, 416, 305–318, 10.1016/j.gca.2025.12.047, 2026.

Overduin, P. P., Wetterich, S., Günther, F., Grigoriev, M. N., Grosse, G., Schirrmeister, L., Hubberten, H.-W., and Makarov, A.: Coastal dynamics and submarine permafrost in shallow water of the central Laptev Sea, East Siberia, The Cryosphere, 10, 1449–1462, 10.5194/tc-10-1449-2016, 2016.

Rachold, V., Grigoriev, M. N., Are, F. E., Solomon, S., Reimnitz, E., Kassens, H., and Antonow, M.: Coastal erosion vs riverine sediment discharge in the Arctic Shelf seas, International Journal of Earth Sciences, 89, 450–460, 10.1007/s005310000113, 2000.

Rasmussen, S. O., Andersen, K. K., Svensson, A. M., Steffensen, J. P., Vinther, B. M., Clausen, H. B., Siggaard-Andersen, M. L., Johnsen, S. J., Larsen, L. B., Dahl-Jensen, D., Bigler, M., Röthlisberger, R., Fischer, H., Goto-Azuma, K., Hansson, M. E., and Ruth, U.: A new Greenland ice core chronology for the last glacial termination, Journal of Geophysical Research: Atmospheres, 111, D06102, 10.1029/2005jd006079, 2006.

Reimer, P. J., Austin, W. E. N., Bard, E., Bayliss, A., Blackwell, P. G., Bronk Ramsey, C., Butzin, M., Cheng, H., Edwards, R. L., Friedrich, M., Grootes, P. M., Guilderson, T. P., Hajdas, I., Heaton, T. J., Hogg, A. G., Hughen, K. A., Kromer, B., Manning, S. W., Muscheler, R., Palmer, J. G., Pearson, C., van der Plicht, J., Reimer, R. W., Richards, D. A., Scott, E. M., Southon, J. R., Turney, C. S. M., Wacker, L., Adolphi, F., Büntgen, U., Capano, M., Fahrni, S. M., Fogtmann-Schulz, A., Friedrich, R., Köhler, P., Kudsk, S., Miyake, F., Olsen, J., Reinig, F., Sakamoto, M., Sookdeo, A., and Talamo, S.: The IntCal20 Northern Hemisphere radiocarbon age calibration curve (0–55 cal kBP), Radiocarbon, 62, 725–757, 10.1017/rdc.2020.41, 2020.

Romanovskii, N. N., Hubberten, H.-W., Gavrilov, A. V., Tumskoy, V. E., and Kholodov, A. L.: Permafrost of the east Siberian Arctic shelf and coastal lowlands, Quaternary Science Reviews, 23, 1359–1369, 10.1016/j.quascirev.2003.12.014, 2004.

Schefuß, E., Eglinton, T. I., Spencer-Jones, C. L., Rullkötter, J., De Pol-Holz, R., Talbot, H. M., Grootes, P. M., and Schneider, R. R.: Hydrologic control of carbon cycling and aged carbon discharge in the Congo River basin, Nature Geoscience, 9, 687–690, 10.1038/ngeo2778, 2016.

Schuur, E. A., Bockheim, J., Canadell, J. G., Euskirchen, E., Field, C. B., Goryachkin, S. V., Hagemann, S., Kuhry, P., Lafleur, P. M., and Lee, H.: Vulnerability of permafrost carbon to climate change: Implications for the global carbon cycle, BioScience, 58, 701–714, 10.1641/B580807, 2008.

Schuur, E. A., McGuire, A. D., Schadel, C., Grosse, G., Harden, J. W., Hayes, D. J., Hugelius, G., Koven, C. D., Kuhry, P., Lawrence, D. M., Natali, S. M., Olefeldt, D., Romanovsky, V. E., Schaefer, K., Turetsky, M. R.,

https://doi.org/10.5194/egusphere-2026-4726
Preprint. Discussion started: 28 August 2026

Treat, C. C., and Vonk, J. E.: Climate change and the permafrost carbon feedback, Nature, 520, 171–179, 10.1038/nature14338, 2015.

Schwamborn, G., Rachold, V., and Grigoriev, M. N.: Late Quaternary sedimentation history of the Lena Delta, Quaternary international, 89, 119–134, 2002.

Shadrick, J. R., Rood, D. H., Hurst, M. D., Piggott, M. D., Hebditch, B. G., Seal, A. J., and Wilcken, K. M.: Sea-level rise will likely accelerate rock coast cliff retreat rates, Nature Communications, 13, 7005, 10.1038/s41467-022-34386-3, 2022.

Sigl, M., Fudge, T. J., Winstrup, M., Cole-Dai, J., Ferris, D., McConnell, J. R., Taylor, K. C., Welten, K. C., Woodruff, T. E., Adolphi, F., Bisiaux, M., Brook, E. J., Buizert, C., Caffee, M. W., Dunbar, N. W., Edwards, R., Geng, L., Iverson, N., Koffman, B., Layman, L., Maselli, O. J., McGwire, K., Muscheler, R., Nishiizumi, K., Pasteris, D. R., Rhodes, R. H., and Sowers, T. A.: The WAIS Divide deep ice core WD2014 chronology – Part 2: Annual-layer counting (0–31 ka BP), Climate of the Past, 12, 769–786, 10.5194/cp-12-769-2016, 2016.

Simon, Q., Thouveny, N., Bourlès, D. L., Valet, J.-P., and Bassinot, F.: Cosmogenic 10Be production records reveal dynamics of geomagnetic dipole moment (GDM) over the Laschamp excursion (20–60 ka), Earth and Planetary Science Letters, 550, 116547, 10.1016/j.epsl.2020.116547, 2020.

Sinnl, G., Adolphi, F., Christl, M., Welten, K. C., Woodruff, T., Caffee, M., Svensson, A., Muscheler, R., and Rasmussen, S. O.: Synchronizing ice-core and U/Th timescales in the Last Glacial Maximum using Hulu Cave 14C and new 10Be measurements from Greenland and Antarctica, Climate of the Past, 19, 1153–1175, 10.5194/cp-19-1153-2023, 2023.

Spielhagen, R., Erlenkeuser, H., and Siegert, C.: History of freshwater runoff across the Laptev Sea (Arctic) during the last deglaciation, Global and Planetary Change, 48, 187–207, 10.1016/j.gloplacha.2004.12.013, 2005.

Stein, R. and Fahl, K.: Holocene accumulation of organic carbon at the Laptev Sea continental margin (Arctic Ocean): Sources, pathways, and sinks, Geo-Marine Letters, 20, 27–36, 2000.

Stein, R. and Fahl, K.: The Laptev Sea: Distribution, sources, variability and burial of organic carbon, in: The organic carbon cycle in the Arctic Ocean, edited by: Stein, R., and MacDonald, R. W., Springer-Verlag, Berlin, 213–237, https://doi.org/10.1007/978-3-642-18912-8, 2004.

Stendel, M. and Christensen, J. H.: Impact of global warming on permafrost conditions in a coupled GCM, Geophysical Research Letters, 29, 10–11, 10.1029/2001gl014345, 2002.

Strauss, J., Schirrmeister, L., Mangelsdorf, K., Eichhorn, L., Wetterich, S., and Herzschuh, U.: Organic-matter quality of deep permafrost carbon – a study from Arctic Siberia, Biogeosciences, 12, 2227–2245, 10.5194/bg-12-2227-2015, 2015.

Strauss, J., Fuchs, M., Hugelius, G., Miesner, F., Nitze, I., Opfergelt, S., Schuur, E., Treat, C., Turetsky, M., Yang, Y., and Grosse, G.: Organic matter storage and vulnerability in the permafrost domain, in: Encyclopedia of Quaternary Science, 399–410, 10.1016/b978-0-323-99931-1.00164-1, 2025.

Strauss, J., Schirrmeister, L., Grosse, G., Fortier, D., Hugelius, G., Knoblauch, C., Romanovsky, V., Schädel, C., Schneider von Deimling, T., Schuur, E. A. G., Shmelev, D., Ulrich, M., and Veremeeva, A.: Deep Yedoma permafrost: A synthesis of depositional characteristics and carbon vulnerability, Earth-Science Reviews, 172, 75–86, 10.1016/j.earscirev.2017.07.007, 2017.

Strauss, J., Laboor, S., Fedorov, A. N., Fortier, D., Froese, D. G., Fuchs, M., Grosse, G., Günther, F., Harden, J. W., Hugelius, G., Kanevskiy, M. Z., Kholodov, A. L., Kunitsky, V. V., Kraev, G., Lapointe-Elmrabti, L., Lozhkin, A. V., Rivkina, E., Robinson, J., Schirrmeister, L., Shmelev, D., Shur, Y., Siegert, C., Spektor, V., Ulrich, M., Vartanyan, S. L., Veremeeva, A., Walter Anthony, K. M., and Zimov, S. A.: Database of Ice-Rich Yedoma Permafrost (IRYP) [dataset], https://doi.org/10.1594/PANGAEA.861733, 2016.

Strauss, J., Laboor, S., Schirrmeister, L., Fedorov, A. N., Fortier, D., Froese, D., Fuchs, M., Günther, F., Grigoriev, M., Harden, J., Hugelius, G., Jongejans, L. L., Kanevskiy, M., Kholodov, A., Kunitsky, V., Kraev, G., Lozhkin, A., Rivkina, E., Shur, Y., Siegert, C., Spektor, V., Streletskaya, I., Ulrich, M., Vartanyan, S.,

https://doi.org/10.5194/egusphere-2026-4726
Preprint. Discussion started: 28 August 2026

Veremeeva, A., Anthony, K. W., Wetterich, S., Zimov, N., and Grosse, G.: Circum-Arctic map of the Yedoma permafrost domain, Frontiers in Earth Science, 9, 758360, 10.3389/feart.2021.758360, 2021.

Strauss, J., Laboor, S., Schirrmeister, L., Fedorov, A. N., Fortier, D., Froese, D. G., Fuchs, M., Günther, F., Grigoriev, M. N., Harden, J. W., Hugelius, G., Jongejans, L. L., Kanevskiy, M. Z., Kholodov, A. L., Kunitsky, V., Kraev, G., Lozhkin, A. V., Rivkina, E., Shur, Y., Siegert, C., Spektor, V., Streletskaya, I., Ulrich, M., Vartanyan, S. L., Veremeeva, A., Walter Anthony, K. M., Wetterich, S., Zimov, N. S., and Grosse, G.: Database of Ice-Rich Yedoma Permafrost Version 2 (IRYP v2), PANGAEA [dataset], 10.1594/PANGAEA.940078, 2022.

Sun, S., Meyer, V. D., Dolman, A. M., Winterfeld, M., Hefter, J., Dummann, W., McIntyre, C., Montluçon, D. B., Haghipour, N., Wacker, L., Gentz, T., van der Voort, T. S., Eglinton, T. I., and Mollenhauer, G.: 14C blank assessment in small-scale compound-specific radiocarbon analysis of lipid biomarkers and lignin phenols, Radiocarbon, 62, 207–218, 10.1017/rdc.2019.108, 2020.

Taldenkova, E., Bauch, H. A., Stepanova, A., Ovsepyan, Y., Pogodina, I., Klyuvitkina, T., and Nikolaev, S.: Benthic and planktic community changes at the North Siberian margin in response to Atlantic water mass variability since last deglacial times, Marine Micropaleontology, 96-97, 13–28, 10.1016/j.marmicro.2012.06.007, 2012.

Taldenkova, E., Bauch, H. A., Gottschalk, J., Nikolaev, S., Rostovtseva, Y., Pogodina, I., Ovsepyan, Y., and Kandiano, E.: History of ice-rafting and water mass evolution at the northern Siberian continental margin (Laptev Sea) during Late Glacial and Holocene times, Quaternary Science Reviews, 29, 3919–3935, 10.1016/j.quascirev.2010.09.013, 2010.

Tesi, T., Muschitiello, F., Smittenberg, R. H., Jakobsson, M., Vonk, J. E., Hill, P., Andersson, A., Kirchner, N., Noormets, R., Dudarev, O., Semiletov, I., and Gustafsson, Ö.: Massive remobilization of permafrost carbon during post-glacial warming, Nature Communications, 7, 13653, 10.1038/ncomms13653, 2016.

Treat, C. C., Jones, M. C., Brosius, L., Grosse, G., Walter Anthony, K., and Frolking, S.: The role of wetland expansion and successional processes in methane emissions from northern wetlands during the Holocene, Quaternary Science Reviews, 257, 106864, 10.1016/j.quascirev.2021.106864, 2021.

Treat, C. C., Kleinen, T., Broothaerts, N., Dalton, A. S., Dommain, R., Douglas, T. A., Drexler, J. Z., Finkelstein, S. A., Grosse, G., Hope, G., Hutchings, J., Jones, M. C., Kuhry, P., Lacourse, T., Lahteenoja, O., Loisel, J., Notebaert, B., Payne, R. J., Peteet, D. M., Sannel, A. B. K., Stelling, J. M., Strauss, J., Swindles, G. T., Talbot, J., Tarnocai, C., Verstraeten, G., Williams, C. J., Xia, Z., Yu, Z., Valiranta, M., Hattestrand, M., Alexanderson, H., and Brovkin, V.: Widespread global peatland establishment and persistence over the last 130,000 y, Proceedings of the National Academy of Sciences of the United States of America, 116, 4822–4827, 10.1073/pnas.1813305116, 2019.

Turetsky, M. R., Abbott, B. W., Jones, M. C., Anthony, K. W., Olefeldt, D., Schuur, E. A. G., Grosse, G., Kuhry, P., Hugelius, G., Koven, C., Lawrence, D. M., Gibson, C., Sannel, A. B. K., and McGuire, A. D.: Carbon release through abrupt permafrost thaw, Nature Geoscience, 13, 138–143, 10.1038/s41561-019-0526-0, 2020.

van Dongen, B. E., Semiletov, I., Weijers, J. W. H., and Gustafsson, Ö.: Contrasting lipid biomarker composition of terrestrial organic matter exported from across the Eurasian Arctic by the five great Russian Arctic rivers, Global Biogeochemical Cycles, 22, GB1011, 10.1029/2007gb002974, 2008.

van Everdingen, R. O., van Everdingen, R. O. (Ed.): Multi-language glossary of permafrost and related ground-ice terms, International Permafrost Association, Calgary, Alberta, Canada, 159 pp.2005.

von Blanckenburg, F. and Bouchez, J.: River fluxes to the sea from the ocean's 10Be/9Be ratio, Earth and Planetary Science Letters, 387, 34–43, 10.1016/j.epsl.2013.11.004, 2014.

Vonk, J. E. and Gustafsson, Ö.: Calibrating n-alkane Sphagnum proxies in sub-Arctic Scandinavia, Organic Geochemistry, 40, 1085–1090, 10.1016/j.orggeochem.2009.07.002, 2009.

https://doi.org/10.5194/egusphere-2026-4726
Preprint. Discussion started: 28 August 2026

Vonk, J. E., Semiletov, I. P., Dudarev, O. V., Eglinton, T. I., Andersson, A., Shakhova, N., Charkin, A., Heim, B., and Gustafsson, Ö.: Preferential burial of permafrost-derived organic carbon in Siberian-Arctic shelf waters, Journal of Geophysical Research: Oceans, 119, 8410–8421, 10.1002/2014jc010261, 2014.

Vonk, J. E., Sanchez-Garcia, L., van Dongen, B. E., Alling, V., Kosmach, D., Charkin, A., Semiletov, I. P., Dudarev, O. V., Shakhova, N., Roos, P., Eglinton, T. I., Andersson, A., and Gustafsson, Ö.: Activation of old carbon by erosion of coastal and subsea permafrost in Arctic Siberia, Nature, 489, 137–140, 10.1038/nature11392, 2012.

Wacker, L. and Christl, M.: Data reduction for small radiocarbon samples–error propagation using the model of constant contamination, in: Ion Beam Physics, ETH Zurich, Annual Report 2011, Laboratory of Ion Beam Physics, ETH Zurich, Zurich, 36–37, 2011.

Winterfeld, M., Mollenhauer, G., Dummann, W., Kohler, P., Lembke-Jene, L., Meyer, V. D., Hefter, J., McIntyre, C., Wacker, L., Kokfelt, U., and Tiedemann, R.: Deglacial mobilization of pre-aged terrestrial carbon from degrading permafrost, Nature Communications, 9, 3666, 10.1038/s41467-018-06080-w, 2018.

Wu, J., Mollenhauer, G., Stein, R., Kohler, P., Hefter, J., Fahl, K., Grotheer, H., Wei, B., and Nam, S. I.: Deglacial release of petrogenic and permafrost carbon from the Canadian Arctic impacting the carbon cycle, Nature Communications, 13, 7172, 10.1038/s41467-022-34725-4, 2022.

Yu, Z., Loisel, J., Brosseau, D. P., Beilman, D. W., and Hunt, S. J.: Global peatland dynamics since the Last Glacial Maximum, Geophysical Research Letters, 37, L13402, 10.1029/2010gl043584, 2010.

Zhang, T., Li, D., East, A. E., Walling, D. E., Lane, S., Overeem, I., Beylich, A. A., Koppes, M., and Lu, X.: Warming-driven erosion and sediment transport in cold regions, Nature Reviews Earth & Environment, 3, 832–851, 10.1038/s43017-022-00362-0, 2022.